

Asteroid Flyby Cyclers Trajectory Design Using Deep Neural Networks

Naoya Ozaki*

Japan Aerospace Exploration Agency, Sagamihara, Kanagawa, 252-5210, Japan

Kanta Yanagida[†], Takuya Chikazawa[‡]

The University of Tokyo, Tokyo 113-8654, Japan

Nishanth Pushparaj[§]

SOKENDAI, Sagamihara, Kanagawa, 252-5210, Japan

Naoya Takeishi[¶]

University of Applied Sciences and Arts Western Switzerland, 1227 Carouge, Switzerland

Ryuki Hyodo^{||}

Japan Aerospace Exploration Agency, Sagamihara, Kanagawa, 252-5210, Japan

Asteroid exploration has been attracting more attention in recent years. Nevertheless, we have just visited tens of asteroids while we have discovered more than one million bodies. As our current observation and knowledge should be biased, it is essential to explore multiple asteroids directly to better understand the remains of planetary building materials. One of the mission design solutions is utilizing asteroid flyby cyclers trajectories with multiple Earth gravity assists. An asteroid flyby cycler trajectory design problem is a subclass of global trajectory optimization problems with multiple flybys, involving a trajectory optimization problem for a given flyby sequence and a combinatorial optimization problem to decide the sequence of the flybys. As the number of flyby bodies grows, the computation time of this optimization problem expands maliciously. This paper presents a new method to design asteroid flyby cycler trajectories utilizing a surrogate model constructed by deep neural networks approximating trajectory optimization results. Since one of the bottlenecks of machine learning approaches is the heavy computation time to generate massive trajectory databases, we propose an efficient database generation strategy by introducing pseudo-asteroids satisfying the Karush-Kuhn-Tucker conditions. The numerical result applied to JAXA's DESTINY⁺ mission shows that the proposed method is practically applicable to space mission design and can significantly reduce the computational time for searching asteroid flyby sequences.

Nomenclature

\mathbf{a}	=	Keplerian orbital elements
a	=	semi-major axis, km
e	=	eccentricity
i	=	inclination, rad

*Ph.D., Assistant Professor, Department of Spacecraft Engineering, Japan Aerospace Exploration Agency, Kanagawa 252-5210, Japan; ozaki.naoya@jaxa.jp, and Member AIAA.

[†]Ph.D. Student, Department of Aeronautics and Astronautics, the University of Tokyo, 7-3-1, Hongo, Bunkyo-ku, Tokyo, 113-8656, Japan.

[‡]Ph.D. Student, Department of Advanced Energy, the University of Tokyo, 7-3-1, Hongo, Bunkyo-ku, Tokyo, 113-8654, Japan.

[§]Ph.D. Student, Department of Space and Astronautical Science, The Graduate University for Advanced Studies, SOKENDAI, Sagamihara, Kanagawa, 252-5210, Japan.

[¶]Ph.D., Postdoctoral Researcher, Geneva School of Business Administration, University of Applied Sciences and Arts Western Switzerland, 1227 Carouge, Switzerland; naoya.takeishi@hesge.ch.

^{||}Ph.D., International Top Young Research Fellow, Department of Solar System Sciences, Japan Aerospace Exploration Agency, Kanagawa 252-5210, Japan.

Ω	=	longitude of the ascending node, rad
$\Delta\Omega$	=	difference of the asteroid Ω from the Earth departure longitude, rad
ω	=	argument of perihelion, rad
M_{epoch}	=	mean anomaly at the epoch, rad
λ	=	longitude, rad
\mathbf{r}	=	position vector, km
\mathbf{v}	=	velocity vector, km/s
\mathbf{v}_{∞}	=	hyperbolic excess velocity vector with respect to the Earth, km/s
m	=	integer number of Earth full revolution; $m \in \mathbb{Z}_{\geq 0}$
n	=	integer number of spacecraft full revolution; $n \in \mathbb{Z}_{\geq 0}$
α	=	pump angle, rad; $\alpha \in [0, \pi]$
κ	=	crank angle, rad; $\kappa \in [0, 2\pi)$
T	=	time of flight, sec
Δv	=	magnitude of impulsive velocity change, km/s
μ	=	gravitational parameter, km^3/s^2
Subscripts		
UB	=	upper bound
LB	=	lower bound
in	=	incoming
out	=	outgoing
sc	=	spacecraft
\odot	=	sun
\oplus	=	Earth
\star	=	asteroid

I. Introduction

Multiple asteroid flyby missions place new scientific constraints on, e.g., chemical, spectral, and geomorphological diversities among asteroids by in-situ surface observations. One of the mission design solutions to visit many asteroids is using asteroid flyby cyclers trajectories[1], a special case of free-return cyclers. Free-return cyclers are periodic trajectories that shuttle a spacecraft between two or more celestial bodies and are typically used in the Sun-Earth-Mars system[2, 3] and planetary moon systems[4, 5]. Unlike typical free-return cyclers, asteroid flyby cyclers do not require the periodicity of all associated bodies' relative geometry because the spacecraft targets different bodies after each Earth gravity assist. An asteroid flyby cycler trajectory design problem addressed in this paper is a subclass of global trajectory optimization problems with multiple flybys and gravity assists, which has attracted many mission designers as one of the most challenging problems.

Global trajectory optimization problems with multiple flybys essentially involve two optimization problems: a nonlinear optimal control problem that optimizes the trajectory for a given flyby sequence and a combinatorial optimization problem to choose the sequence of the flybys. Recent studies have proposed global trajectory optimization methods utilizing population-based metaheuristics[6–8], a binary tree search[9], and indirect methods[10, 11]. Englander et al. have applied their evolutionary algorithm-based method to NASA's Lucy mission, which visits multiple Trojan asteroids[1]. Sánchez Cuartielles et al. and Bowles et al. have studied multiple-flyby trajectory design methods via genetic algorithm for the CASTAway mission[12, 13]. Although metaheuristic approaches are successfully implemented for practical missions, the approaches face computational difficulties when the number of target bodies grows. We need further studies to search for target asteroids among the million of them comprehensively. As a post-analysis discussion, Englander et al. have also remarked a trend among orbital elements ω and Ω of accessible asteroids[1]. This trend indicates that embedding a well-designed surrogate model into a global trajectory optimization process enables us to search for accessible asteroids efficiently.

In machine learning and optimization theory, researchers have studied efficient global optimization algorithms utilizing surrogate models[14]. A surrogate model is a black-box model that approximates the relationship between inputs and outputs rather than calculates it directly. We can rapidly obtain the global optimal solution by replacing time-consuming trajectory optimization with a less time-consuming surrogate model constructed by a neural network. One of the most successful examples is Bayesian optimization[15], which commonly uses a Gaussian process as a surrogate model. This method is widely used to tune hyperparameters of machine learning[16]. Some of the other

methods implement surrogate models in an evolutionary algorithm[17] and particle swarm optimization[18]. In recent years, astrodynamics researchers have started applying machine learning techniques to space mission design[19–21], and some of them have presented surrogate-assisted global trajectory optimization methods[22–28]. Their surrogate models, made by classical regression method[22, 23], Gaussian processes[24, 25], Deep Neural Networks (DNNs)[26–29], approximate the cost function of the nonlinear trajectory optimization problem and let us evaluate the cost quickly without solving the trajectory optimization problems. Although the DNN-based method accurately approximates the actual cost function, for example, multiple rendezvous missions with near-Earth asteroids (NEAs)[26], its training requires a computationally expensive massive database (e.g., hundreds of thousands of optimal trajectories). Izzo and Öztürk[29] have studied an innovative approach that generates a massive database efficiently without solving trajectory optimization problems directly, yet this prior study is only applicable to low-thrust controllers for two-point boundary value problems such as the Earth-Venus transfer.

This paper presents a novel method to design asteroid flyby cyclers trajectories utilizing a surrogate model constructed by DNNs. Our approach builds the surrogate model of nonlinear trajectory optimization and then efficiently searches for flyby sequences using the tree search method with the surrogate model. Our first contribution is to bring the surrogate-based approach to a practical flyby trajectory design by improving the prediction accuracy of our surrogate model by utilizing astrodynamics knowledge, such as free-return trajectories[4, 30–32] and Lambert’s problem[33]. The second contribution is to allow the resulting surrogate model to be reusable for different mission scenarios (different Earth departure epoch, hyperbolic excess velocity, and target asteroids) without re-training DNNs by normalizing the dataset with the longitude at the Earth departure epoch. The third contribution is to establish an efficient database generation strategy that can produce multiple datasets from a single trajectory optimization result by introducing pseudo-asteroids while maintaining the optimization condition, the Karush–Kuhn–Tucker (KKT) condition. This strategy can amplify the size of the trajectory optimization database by one order of magnitude by solving a simple algebraic equation. Finally, we search for optimal flyby sequence by a beam search method[34] where the heuristic cost is quickly estimated by utilizing the surrogate model. Our proposed approach is tested in the numerical application to JAXA’s DESTINY+ mission[35] performing multiple asteroid flybys, including (3200) Phaethon.

II. Background

This section provides the necessary definition of the dynamics, free-return trajectories, and the trajectory optimization problem, including the assumptions and the notation. Our goal is to fly by as many scientifically interesting asteroids as possible within the limited spacecraft capability (propellant and lifetime). In particular, we assume that the fuel constraints are severe, while the requirements on lifetime are relatively loose. To this end, we utilize Earth gravity-assist maneuvers repeatedly, achieved by the Earth free-return trajectories, as shown in Fig.1. This approach reduces the total fuel consumption significantly with a relatively long time of flight.

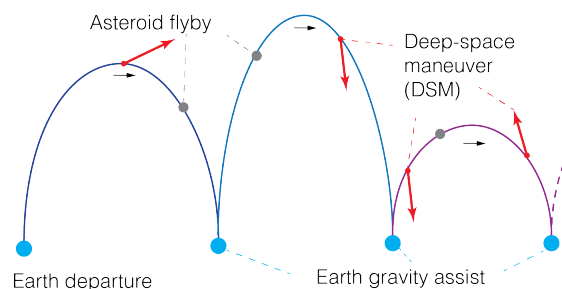


Fig. 1 Asteroid flyby cycler.

A. Dynamics and Models

We consider that the dynamics of spacecraft, asteroids, and the Earth are governed only by the sun’s gravity, and the Earth is moving in a circular orbit on the ecliptic plane, known as the zero-radius sphere-of-influence patched-conics model[36, 37]. The Earth gravity assist is modeled as an instantaneous velocity change at the intersection of the spacecraft and the Earth’s orbits. We describe the spacecraft heliocentric state via Cartesian elements $\mathbf{x} = [\mathbf{r}^T, \mathbf{v}^T]^T$.

The equation of motion of the spacecraft is described as follows:

$$\frac{d}{dt} \begin{bmatrix} \mathbf{r} \\ \mathbf{v} \end{bmatrix} = \begin{bmatrix} \mathbf{v} \\ -\frac{\mu_{\odot}}{\|\mathbf{r}\|^3} \mathbf{r} \end{bmatrix} \quad (1)$$

We formulate the trajectory optimization problem via the multiple gravity-assists with one deep-space maneuver (MGA-1DSM) model[6, 36, 38], where a single deep-space maneuver can be performed at any point along the trajectory between each consecutive flybys. Although we demonstrate our algorithm using the MGA-1DSM model, this algorithm can be potentially extended to low-thrust trajectory optimization if the computational time allows.

B. Free-return Trajectories

Our studies investigate asteroid flyby cyclers using Earth free-return trajectories and patching them together with Earth gravity-assist maneuvers. Russell et al.[4, 30] have proposed a systematic method to identify all feasible free-return trajectories under the assumption that the flyby body is moving in a circular orbit. As per their approach, the free-return trajectories fall into three categories shown in Fig.2: 1) full-revolution transfers, 2) half-revolution transfers, and 3) generic transfers. The free-return trajectory can be uniquely determined when the parameters shown in Table 1 are fixed. Introducing the v-infinity globe[39], we can plot all free-return trajectories as points on the globe as shown in Fig.3. In Fig.3, the red large circles represent the v-infinity direction of the full revolution free-return trajectories; the blue markers indicate the half revolution trajectories; the green dots indicate the generic free-return trajectories. Details for calculating all free-return trajectories can be found in Ref.[4, 30–32].

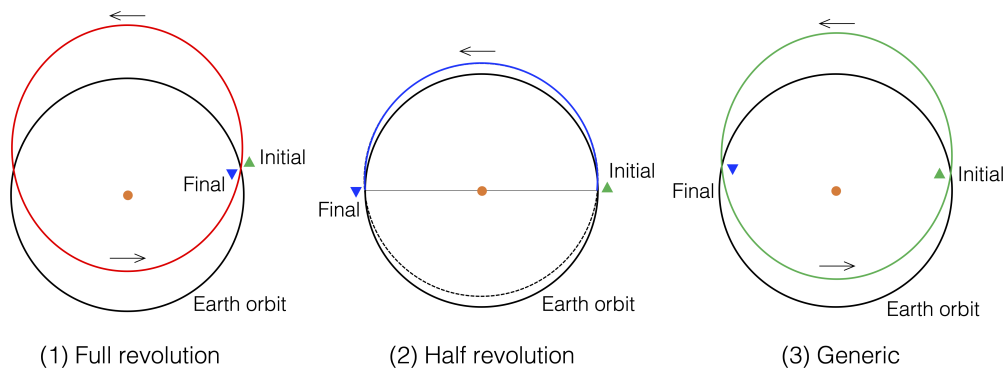


Fig. 2 Three category of free-return trajectories.

Table 1 Parameters determining free-return trajectories

Type	Continuous	Discrete
full	$v_{\infty} \in \mathbb{R}_{\geq 0}, \kappa \in [0, 2\pi)$	$m, n \in \mathbb{Z}_{\geq 0}$
half	$v_{\infty} \in \mathbb{R}_{\geq 0}$	$m, n \in \mathbb{Z}_{\geq 0}, \{\text{inbound, outbound}\}, \{\text{above, below}\}$
generic	$v_{\infty} \in \mathbb{R}_{\geq 0}$	$m, n \in \mathbb{Z}_{\geq 0}, \{\text{inbound, outbound}\}, \{\text{direct, retrograde}\}$

C. Asteroid Flyby Cyclers Trajectory Design Problem

We formulate the asteroid flyby cycler trajectory design problem by dividing the whole problem into smaller subproblems[34]. One of them is an Earth-asteroid-Earth trajectory optimization problem under the MGA-1DSM models to construct the Earth-asteroid-Earth block. The other subproblem is to search the sequence of target asteroids via tree searches. Although this greedy formulation only yields a series of optimal trajectories that approximate the global optimal trajectory, this simplification allows us to demonstrate surrogate-based flyby trajectory design with practical resources. We also insert Earth free-return transfers without visiting any asteroids if needed (mainly for changing Earth flyby longitude). Visiting more than one asteroid between each Earth-to-Earth leg is out of the main

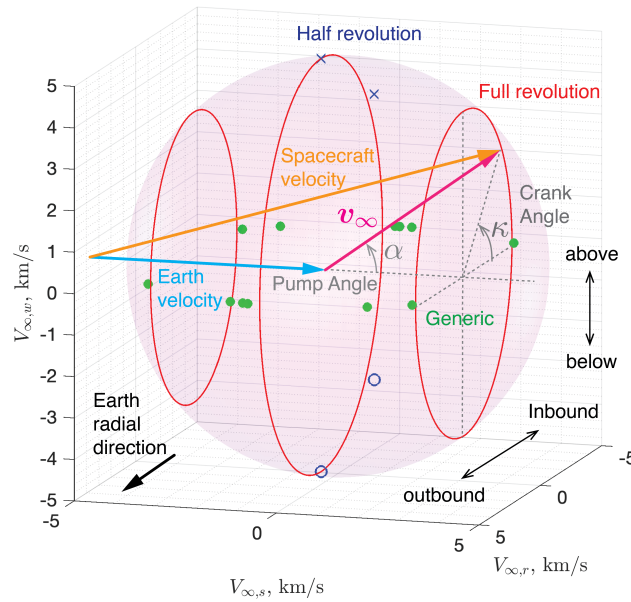


Fig. 3 The v -infinity globe of Earth free-return trajectories ($V_{\infty} = 5\text{km/s}$ and $m \leq 3$), where s axis along the velocity vector of the flyby body, w axis along the angular momentum vector of the flyby body, and r axis completes the right-handed system.

scope of this research. Once the sequence of asteroid flybys is determined, we optimize the patched trajectory and evaluate the total ΔV consumption and the total time of flight.

1. Earth-Asteroid-Earth Block

We formulate the Earth-asteroid-Earth transfer problems by two consecutive MGA-1DSM models, where the gravities of asteroids are ignored, as shown in Fig.4. The main task of this subproblem is to calculate the optimal Earth-asteroid-Earth transfers that minimize the total ΔV (the sum of DSM1 and DSM2). Initial epoch t_0 and initial v -infinity magnitude $v_{\infty,0}$ are fixed; final epoch t_f and final v -infinity $v_{\infty,f}$ are free. The spacecraft performs an asteroid flyby during the Earth-to-Earth transfer; that is, the positions of two bodies match at $t_{\star} \in (t_0, t_f) \subset \mathbb{R}$.

The inputs of this block are t_0 , $v_{\infty,0}$, the parameters of free-return trajectory, and the orbital elements of the target asteroid $\mathbf{a} = [a, e, i, \Omega, \omega, M_{t_{0e}}]$. As the outputs of this problem, we obtain the total ΔV consumption, t_f , and $v_{\infty,f}$. Figure 5 illustrates the relationship between the inputs and outputs of the Earth-asteroid-Earth transfer problem.

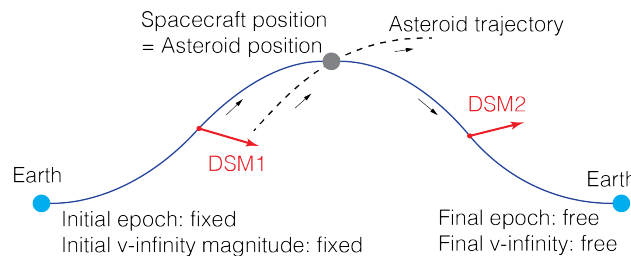


Fig. 4 Definition of Earth-asteroid-Earth trajectory optimization problem.

2. Tree Searches of Flyby Sequence

Using the result of the Earth-asteroid-Earth block, we search for the good sequences of free-return parameters and target asteroids via tree search methods[34]. The tree search parameters are the free-return parameters (m, n, type)

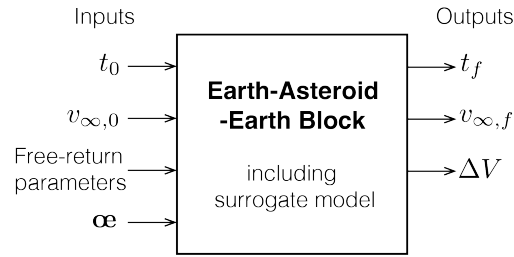


Fig. 5 Inputs and outputs of the Earth-asteroid-Earth block.

and the orbital elements of the asteroids α . Figure 6 illustrates an example sequence where we first select α as the free-return parameter and α_x as the orbital element and then select β as the free-return parameter and α_y as the orbital element. The cost of the flyby sequences depends on the solution of the Earth-asteroid-Earth block, whereas the inputs of the Earth-asteroid-Earth block are given when the flyby sequence is determined. Hence, without the surrogate model, we need to solve trajectory optimization problems to evaluate the cost of the tree nodes.

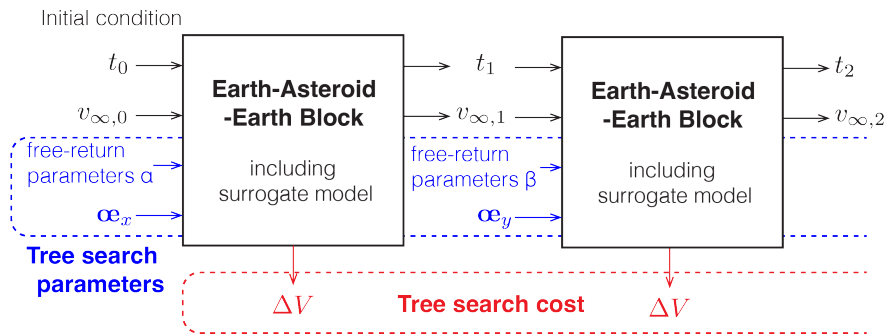


Fig. 6 Flyby sequence tree search using Earth-asteroid-Earth block.

III. Asteroid Flyby Cyler Trajectory Design via Deep Neural Networks

This section presents a novel asteroid flyby cyler design method using the surrogate model constructed via DNNs. Figure 7 illustrates the proposed trajectory design procedure and indicates the corresponding sections. We create the surrogate model of the Earth-asteroid-Earth block that allows us to quickly estimate the cost of each transfer between asteroids without solving trajectory optimization problems during the tree search. Since the DNN-based methods require gigantic databases, we propose an efficient database generation strategy by introducing pseudo-asteroids that spacecraft can fly by in the same optimal trajectory. Finally, we apply beam search using the surrogate model to find good asteroid flyby sequences.

A. Architecture of Earth-Asteroid-Earth Block

In the Earth-asteroid-Earth block, we first generate the free-return trajectories for given parameters (v_{∞} , the number of revolutions, the type classifiers of the free-return trajectories) defined in Table 1. The optimal Earth-asteroid-Earth trajectory exists near an Earth free-return trajectory. In particular, the free-return trajectory will be the optimal trajectory when the asteroid crosses in the free-return trajectory. Using the information of the free-return trajectory, we filter the accessible asteroids through screening algorithms based on a) Lambert's problem or b) closest approach distance from the free-return trajectory. We use the results of the screening algorithms as the initial guess of the trajectory optimization problem, that is, as the inputs of the surrogate model. We build a surrogate model of trajectory optimization because it is the most computationally intensive. Figure 8 illustrates the architecture of the Earth-asteroid-Earth block.

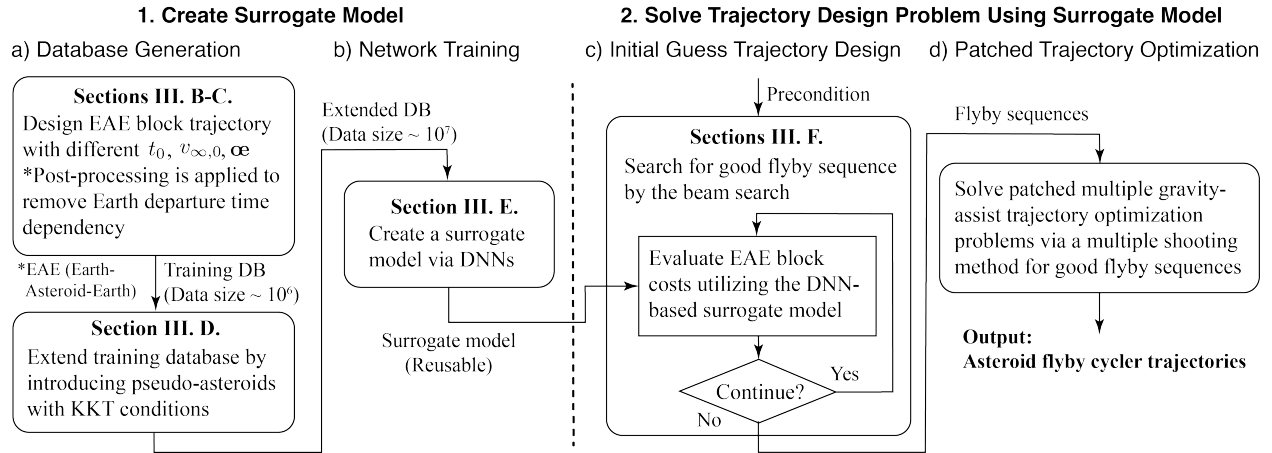


Fig. 7 Surrogate-based asteroid flyby cyclers trajectory design procedure.

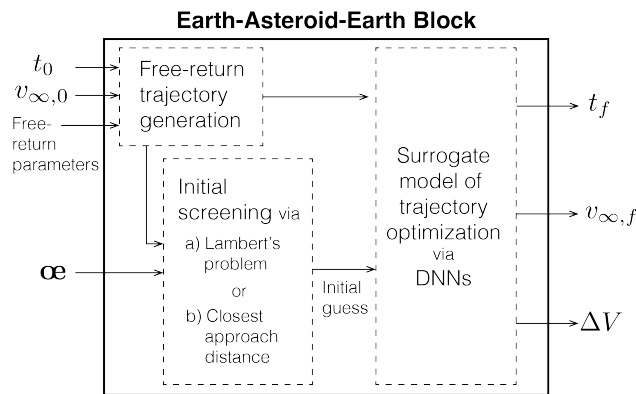


Fig. 8 Architecture of Earth-asteroid-Earth block.

B. Initial Screening Algorithm

We adopt two initial screening algorithms and compare their performance. One method solves Lambert's problem, and the other calculates the closest approach distance from the free-return trajectory.

1. Screening Algorithm by Lambert's Problem

One of the asteroid screening algorithms that we adopt is based on Lambert's problem. We use the stable and fast computational method of Lambert's problem in Ref.[33]. This screening algorithm divides the Earth-asteroid-Earth trajectory into two phases; the first phase is from the Earth to the asteroid, and the second phase is from the asteroid to the Earth. We solve Lambert's problems for each phase by changing the asteroid flyby epoch. The initial and final epochs at the Earth flybys are fixed to the ones of the free-return trajectory. Using a grid search regarding the asteroid flyby epoch, we iteratively solve Lambert's problems to find the optimal flyby epoch, where the step size is 3 days in our numerical example. We choose this step size as small as the computation time allows. Because the computation time of Lambert's problem is not negligible in the proposed architecture, we can likely accelerate the computation by introducing an adaptive step size scheme. The objective function of this grid search is the sum of two ΔV s needed for the transfer. One of the ΔV s is the difference between the initial hyperbolic excess velocity needed for Lambert's transfer and the one we assume for the free-return trajectory. The other ΔV is the velocity difference at the asteroid flyby point between phases. We store the results if the total ΔV is less than a threshold. The threshold is set to 3 km/s in our numerical example.

2. Screening Algorithm by Closest Approach Distance

The other asteroid screening algorithm that we adopt is based on the closest approach distance of the asteroid from an Earth free-return trajectory. In this algorithm, we first propagate a free-return trajectory and all asteroid trajectories. In this propagation, the initial epoch t_0 is given; the final epoch $t_{FR,f}$ is given from the free-return transfer; the time step Δt is a tuned parameter, where Δt is 3 days in our numerical example. For each fraction of the trajectories defined in the time span $(t_j, t_j + \Delta t)$, we calculate the distance $d(t_j)$ between the free-return trajectory and an asteroid trajectory under the uniform linear motion assumption by the following equation

$$d(t_j) = \|\mathbf{r}_{\text{rel}} - \delta t \mathbf{v}_{\text{rel}}\| \quad (2)$$

$$\delta t := \min \left(\max \left(\frac{\mathbf{r}_{\text{rel}} \cdot \mathbf{v}_{\text{rel}}}{\|\mathbf{v}_{\text{rel}}\|^2}, 0 \right), \Delta t \right) \quad (3)$$

where $\mathbf{r}_{\text{rel}} := \mathbf{r}_{\text{sc}}(t_j) - \mathbf{r}_\star(t_j)$, $\mathbf{v}_{\text{rel}} := \mathbf{v}_{\text{sc}}(t_j) - \mathbf{v}_\star(t_j)$. Then, the closest approach distance d_{CA} between the free-return trajectory and the asteroid is calculated by

$$d_{CA} = \min_{t_j \in \mathcal{T}} d(t_j) \quad (4)$$

where $\mathcal{T} := \{t_0 + j\Delta t : j \in \mathbb{N}, t_0 + j\Delta t \in (t_0, t_{FR,f})\}$. We store the results if the closest approach distance d_{CA} is less than a threshold, which is 5,000,000 km in our numerical example.

C. Generating Database of Earth-Asteroid-Earth Optimal Trajectories

We optimize the trajectory via a direct multiple shooting method using the initial guess trajectories produced by the initial screening algorithm. Lambert's solution gives the initial guess trajectory for Lambert's screening, while the free-return trajectory provides the initial guess trajectory for the closest approach screening. Figure 9 illustrates the definition of the trajectory optimization problem. The Earth-asteroid-Earth trajectory is divided into three phases. We introduce 9 optimization variables for each phase, including nodal state vectors $\left[\mathbf{r}_{\text{sc},i}^\top, \mathbf{v}_{\text{sc},i}^\top \right]^\top$ or $\left[\mathbf{v}_{\infty\text{in},i}^\top, \mathbf{v}_{\infty\text{out},i}^\top \right]^\top$, time t_i , backward propagation time $T_{B,i}$, and forward propagation time $T_{F,i}$. The objective function of this trajectory optimization is the sum of ΔV s at the patching points

$$\begin{aligned} J &= \sum_{i=1}^2 \Delta V_i \\ &= \sum_{i=1}^2 \sqrt{\|\mathbf{v}_{B,i} - \mathbf{v}_{F,i-1}\|^2 + \epsilon}, \end{aligned} \quad (5)$$

where $\mathbf{v}_{B,i}$ is the velocity calculated by the backward propagation of phase i ; $\mathbf{v}_{F,i-1}$ is the velocity calculated by the forward propagation of phase $i-1$, and; ϵ is a small number introduced to make the objective function differentiable.

We consider 12 equality constraints defined by the following equations.

$$F_1 = \|\mathbf{v}_{\infty\text{out},0}\| - \bar{v}_{\infty,0} = 0 \quad (6)$$

$$F_2 = (t_0 + T_{F,0}) - (t_1 + T_{B,1}) = 0 \quad (7)$$

$$\mathbf{F}_{3:5} = \mathbf{r}_{B,1} - \mathbf{r}_{F,0} = \mathbf{0} \quad (8)$$

$$\mathbf{F}_{6:8} = \mathbf{r}_{\text{sc},1} - \mathbf{r}_\star(t_1) = \mathbf{0} \quad (9)$$

$$F_9 = (t_1 + T_{F,1}) - (t_2 + T_{B,2}) = 0 \quad (10)$$

$$\mathbf{F}_{10:12} = \mathbf{r}_{B,2} - \mathbf{r}_{F,1} = \mathbf{0} \quad (11)$$

where $\mathbf{r}_{B,i}$ is the position calculated by the backward propagation of phase i ; $\mathbf{r}_{F,i-1}$ is the position calculated by the forward propagation of phase $i-1$; $\bar{v}_{\infty,0}$ is the v-infinity magnitude given as the input of the Earth-asteroid-Earth block, and; $\mathbf{r}_\star(t_1)$ is the position of the asteroid at t_1 calculated from its ephemeris. We bound the optimization variables as

given by the following equations.

$$\mathbf{v}_{\infty in,0} = \mathbf{0} \quad (12)$$

$$t_0 = \bar{t}_0 \quad (13)$$

$$T_{B,0} = 0 \quad (14)$$

$$\mathbf{v}_{\infty out,2} = \mathbf{0} \quad (15)$$

$$t_{FR,f} - 3\text{mos.} \leq t_2 \leq t_{FR,f} + 3\text{mos.} \quad (16)$$

$$T_{F,2} = 0 \quad (17)$$

where \bar{t}_0 is the initial epoch given as the input of the Earth-asteroid-Earth block, and; $t_{FR,f}$ is the final epoch given from the free-return transfer. Finally, the trajectory optimization problem can be described by the form of nonlinear programming (NLP), which can be solved by a sequential quadratic programming (SQP) solver such as SNOPT[40].

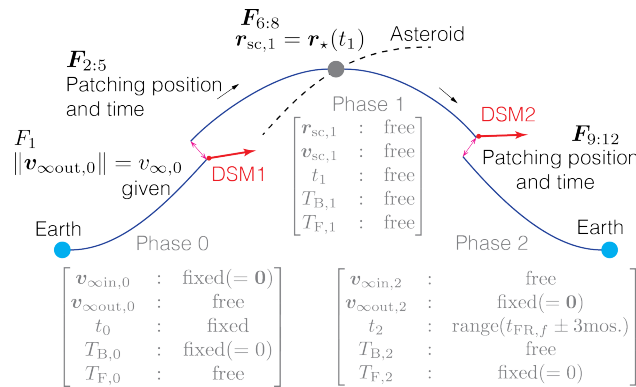


Fig. 9 Definition of trajectory optimization problem via multiple shooting.

The resulting database has a dependency on the initial epoch, i.e., the Earth departure epoch. When we use this database to build a surrogate model, the generalization performance will be insufficient if the Earth departure epoch is outside the range of the database. Therefore, as post-processing, we transform a database that is independent of the Earth departure epoch. As shown in Fig. 10, the orbital elements Ω and M of the asteroid are converted as follows.

$$\begin{cases} \Omega \rightarrow \Delta\Omega_{t_0} := \Omega - \lambda_{\oplus}(t_0) \\ M_{t_{\alpha}} \rightarrow M_{t_0} := M_{t_{\alpha}} + \sqrt{\frac{\mu_{\oplus}}{a^3}}(t_0 - t_{\alpha}) \end{cases} \quad (18)$$

where $\lambda_{\oplus}(t_0)$ is the longitude of the Earth at t_0 , and t_{α} is the epoch at which the orbital element is given. The remaining orbital elements a, e, i, ω are invariant to this transformation. This transformation allows the proposed surrogate model to be applied to any Earth departure epoch.

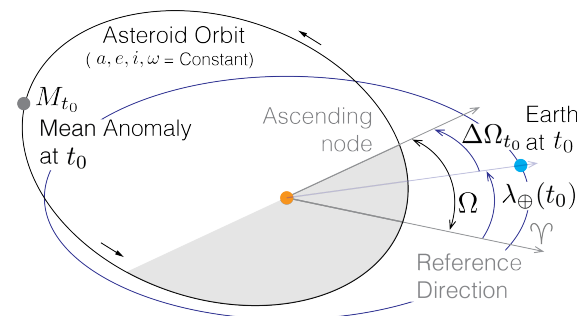


Fig. 10 Definition of $\Delta\Omega$ and mean anomaly at t_0 .

D. Extension of Database with Pseudo Asteroid under KKT conditions

Since the database generation by trajectory optimization is computationally expensive, we propose a new database generation strategy by introducing pseudo-asteroids that can be flown by spacecraft in the same optimal trajectory. The spacecraft can fly by a pseudo-asteroid if the pseudo-asteroid crosses the spacecraft's trajectory. However, this crossing condition does not guarantee the optimality of this trajectory to the pseudo-asteroid. In order to ensure the optimality of the trajectory, the pseudo-asteroid must satisfy the optimality conditions, also known as the KKT conditions. The proposed approach generates pseudo-asteroids for each optimal trajectory, for which we have already computed all optimization variables and Lagrange multipliers.

The optimal trajectory satisfies the following constraint at the flyby point

$$\mathbf{F}_{6:8} = \mathbf{r}_{sc,1} - \mathbf{r}_\star(t_1) = \mathbf{0}$$

Let us assume that a pseudo-asteroid intersects the optimized trajectory at t_1 . Then, the position of the pseudo-asteroid $\mathbf{r}_{p\star}$ can be computed as follows.

$$\mathbf{r}_{p\star}(t_1) = \mathbf{r}_\star(t_1) = \mathbf{r}_{sc,1} \quad (19)$$

The velocity of the pseudo-asteroid $\mathbf{v}_{p\star}$ is determined through the conservation of the KKT conditions. Because all optimization variables and Lagrange multipliers maintain the same value, the following terms of the KKT conditions must be satisfied.

$$\lambda_{6:8}^\top \frac{\partial \mathbf{F}_{6:8}}{\partial t_1} = \lambda_{6:8}^\top \{-\mathbf{v}_\star(t_1)\} = \lambda_{6:8}^\top \{-\mathbf{v}_{p\star}(t_1)\} \quad (20)$$

Hence,

$$\lambda_{6:8}^\top \{\mathbf{v}_{p\star}(t_1) - \mathbf{v}_\star(t_1)\} = 0 \quad (21)$$

Note that the velocity vector of the pseudo-asteroid $\mathbf{v}_{p\star}$ has two degrees of freedom.

We can determine the velocity of the pseudo-asteroids by introducing two random variables \mathbf{v}_{rand} and α_{rand} . The first step computes a vector perpendicular to $\lambda_{6:8}$.

$$\mathbf{v}_{\star\perp} = \mathbf{v}_{rand} - \frac{\lambda_{6:8}^\top \mathbf{v}_{rand}}{\|\lambda_{6:8}\|^2} \lambda_{6:8} \quad (22)$$

The second step calculates the velocity of the pseudo-asteroid as the following equation.

$$\mathbf{v}_{p\star}(t_1) = \mathbf{v}_\star(t_1) + \alpha_{rand} \mathbf{v}_{\star\perp} \quad (23)$$

The relation among \mathbf{v}_\star , $\mathbf{v}_{p\star}$, $\lambda_{6:8}$, and $\mathbf{v}_{\star\perp}$ is illustrated in Fig. 11. In the numerical results, we set up the bound on the semi-major axis of the pseudo-asteroid. Therefore, α_{rand} is decided so that $\mathbf{v}_{p\star}$ satisfies

$$a_{LB} \leq \left(\frac{2}{\|\mathbf{r}_{p\star}\|} - \frac{\|\mathbf{v}_{p\star}\|^2}{\mu_\odot} \right)^{-1} \leq a_{UB}. \quad (24)$$

We can finally calculate the Keplerian orbital elements of the pseudo-asteroid \mathbf{a}_p from the Cartesian state vector $(\mathbf{r}_{p\star}, \mathbf{v}_{p\star})$ at the epoch t_1 . If we generate 10 pseudo-asteroids for each optimal trajectory, the proposed method can expand the size of the database about 11 times.

E. Surrogate Model by Deep Neural Networks

We create the surrogate model by the DNNs regression using the massive databases of the optimal trajectories. In this work we use a feed-forward neural network with fully-connected layers, and hyperparameters such as the number of layers M , the number of units N , and the learning rate ϵ are selected through the sensitivity analysis. Activation functions of the first $(M - 1)$ layers are exponential linear units (ELUs)[41] and of the last one is sigmoid to handle the bounded outputs. We add a dropout or a one-dimensional batch normalization [42] layer after each of the first $(M - 1)$ layers. The dropout layer is to prevent over-fitting and the batch normalization layer is to improve stability.

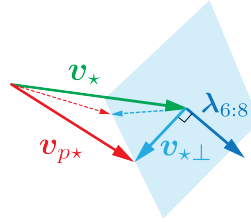


Fig. 11 Pseudo-asteroid velocity.

The inputs and outputs of the regression model are shown in Tables 2 and 3. The details of the input information are explained in Appendix A. We apply two operations to the outputs in order to improve the performance of the regression. The first operation calculates the difference of t_f and $v_{\infty,f}$ from the values of the free-return trajectories. That is,

$$\begin{cases} \Delta t_f &= t_f - t_{fFR} \\ \Delta v_{\infty,f} &= v_{\infty,f} - v_{\infty,fFR}. \end{cases} \quad (25)$$

where t_{fFR} and $v_{\infty,fFR}$ are respectively the final epoch and hyperbolic excess velocity of the free-return trajectory calculated from $(m, n, \text{type}, v_{\infty,0})$. Note that we do not apply this operation to ΔV because ΔV of the free-return trajectory is zero. This operation lets $\Delta \mathbf{z} (= [\Delta t_f, \Delta v_{\infty,f}, \Delta V]^T)$ be distributed around zero. The second operation takes $\tan^{-1}(\cdot)$ for each element of $\Delta \mathbf{z}$. $\tan^{-1}(\cdot)$ provides a soft bound on the output and increases the sensitivity to values close to zero. Although $\Delta \mathbf{z}$ are unbound, the ranges of interest are fixed. For example, a trajectory design with $\Delta V = 10$ km/s (out of the range of interest) usually does not require an accurate ΔV prediction. Finally, the outputs \mathcal{Y}_{z_i} of DNNs are calculated as

$$\mathcal{Y}_{z_i} = \tan^{-1}(\Delta z_i / \chi_{z_i}) \quad (26)$$

where

$$\chi_{z_i} = \Delta z_{i,90\%} \cdot \tan\left(\frac{0.9\pi}{2}\right) \quad (27)$$

where Δz_i is an element of $\Delta \mathbf{z}$, and $\Delta z_{i,90\%}$ is a user-defined parameter.

For the stability of the training, input variables except for m , n , and "type" are normalized to a standard normal distribution and all output variables are re-scaled to $[0, 1]$. About exceptions, m and n are used as is, and "type" is converted to an integer.

Table 2 Inputs and outputs of DNNs (screened by Lambert's problem)

Inputs	Outputs
Free-return info $(m, n, \text{type}, v_{\infty,0})$	$\tan^{-1}\left(\frac{\Delta t_f}{\chi_{\Delta t_f}}\right)$
Asteroid ephemeris $(a, e, i, \Delta\Omega_{t_0}, \omega, M_{t_0})$	$\tan^{-1}\left(\frac{\Delta v_{\infty,f}}{\chi_{\Delta v_{\infty,f}}}\right)$
ΔV s of Lambert's Method $(\Delta v_0, \Delta v_1, \Delta v_{\text{total}})$	$\tan^{-1}\left(\frac{\Delta V}{\chi_{\Delta V}}\right)$
Initial guess of $T, n_*, \eta_{t_*}, v_{\infty\text{out},0}, v_{\infty\text{in},f}, v_{\text{rel,in},1}$, and $v_{\text{rel,out},1}$	

For training, we divide the entire dataset into minibatches, where the minibatch size is 1024, and update the network parameters for each minibatch. The performance of the networks is evaluated by the mean squared error (MSE) loss

Table 3 Inputs and outputs of DNNs (screened by closest approach distance)

Inputs	Outputs
Free-return info ($m, n, \text{type}, v_{\infty,0}$)	$\tan^{-1} \left(\Delta t_f / \chi_{\Delta t_f} \right)$
Asteroid ephemeris ($a, e, i, \Delta \Omega_{t_0}, \omega, M_{t_0}$)	$\tan^{-1} \left(\Delta v_{\infty,f} / \chi_{\Delta v_{\infty,f}} \right)$
Closest approach state difference ($\delta \mathbf{r}_{CA}$ and $\delta \mathbf{v}_{CA}$)	$\tan^{-1} \left(\Delta V / \chi_{\Delta V} \right)$
Initial guess of $T, n_{\star}, \eta_{t_{\star}}, \mathbf{v}_{\infty,0}, \mathbf{v}_{\infty,f}$, and $\boldsymbol{\alpha}_{FR}$	

defined as follows.

$$\mathcal{L}_{\text{total}} := \mathcal{L}_{\Delta t_f} + \mathcal{L}_{\Delta v_{\infty,f}} + \mathcal{L}_{\Delta V} \quad (28)$$

$$\mathcal{L}_{\Delta t_f} := \frac{1}{3} \left\langle \left(\mathcal{Y}_{\Delta t_f} - \hat{\mathcal{Y}}_{\Delta t_f} \right)^2 \right\rangle \quad (29)$$

$$\mathcal{L}_{\Delta v_{\infty,f}} := \frac{1}{3} \left\langle \left(\mathcal{Y}_{\Delta v_{\infty,f}} - \hat{\mathcal{Y}}_{\Delta v_{\infty,f}} \right)^2 \right\rangle \quad (30)$$

$$\mathcal{L}_{\Delta V} := \frac{1}{3} \left\langle \left(\mathcal{Y}_{\Delta V} - \hat{\mathcal{Y}}_{\Delta V} \right)^2 \right\rangle \quad (31)$$

where $\hat{\cdot}$ is the estimated value by DNNs and we use the notation $\langle \cdot \rangle = (1/N) \sum(\cdot)$ to describe the mean value across the minibatch. The network parameters are optimized to minimize the loss function using Adam[43], a stochastic gradient descent method. We run this training process over multiple epochs, where one epoch is completed when the entire dataset is consumed.

F. Tree Search Method

This paper employs beam search (e.g., [34]) to search for the good sequences of asteroids using the surrogate-based Earth-asteroid-Earth block. Beam search is a heuristic search algorithm that uses breadth-first search in a limited set. At each level of the tree, the algorithm sorts successors by a heuristic cost, the total ΔV evaluated by the surrogate model, and stores only a predetermined number of best states, called the *beam width*. The algorithm also discards the states if the total Time of Flight (TOF) is more than the upper bound (10 years in the numerical example) or the deflection angle of the Earth gravity assist is infeasible (minimum perigee altitude is 500 km in the numerical example). Beam search does not guarantee to find the best solution; however, it is helpful to systematically search the solutions. Figure 12 summarizes the beam search algorithm search for the asteroid flyby sequences. The initial screening algorithm first prunes unpromising solutions before evaluating the heuristic cost.

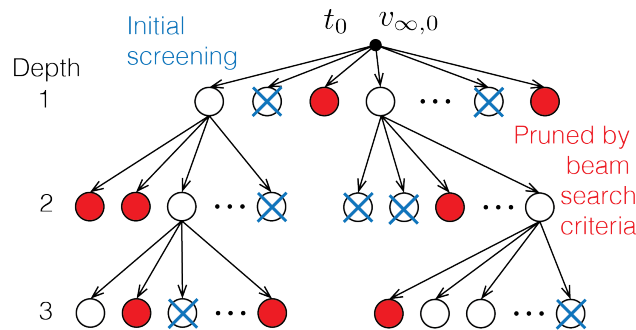


Fig. 12 Beam search method.

IV. Numerical Results

This section applies the proposed method to DESTINY+mission[35], which is JAXA's Epsilon medium-class mission to be launched in 2024. To enable lower cost and higher frequency deep space missions, the spacecraft will demonstrate advanced technologies that include highly efficient solar electric propulsion. For the science mission, the spacecraft will perform high-speed flyby observation and explore the asteroid (3200) Phaethon as the nominal mission and several more asteroids as an extra mission[35, 44, 45]. Figures 13 and 14 respectively show the mission scenario and the baseline trajectories of DESTINY+. In this numerical example, we deal with the extra mission phase that starts with a gravity assist from the Earth after the Phaethon flyby.

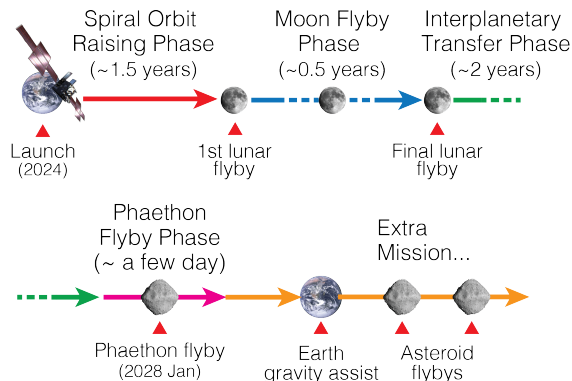


Fig. 13 Mission scenario of DESTINY+.

A. Precondition

DESTINY+ can only approach Phaethon at the vicinity of its descent node on the ecliptic plane because Phaethon's orbit has a large inclination angle and high eccentricity ($i = 22.26\text{deg}$ and $e = 0.88990$). Considering the constraint on the distance to Earth for high-speed communication, the possible flyby timing is limited to either January 2028 (nominal) or November 2030 (backup). In the nominal scenario, the spacecraft returns to the Earth at 2028 MAY 05 12:13:59 TDB with $v_{\infty,0} = 2.684\text{km/s}$. We perform the following numerical simulations under this initial condition.

B. Training Database

We created multiple databases of the Earth-asteroid-Earth optimal trajectories (with each screening algorithm, with or without the pseudo-asteroids) and compared the performance of the surrogate models trained on each database. Table 4 summarizes the definition of the database. Cases 2, 3, 5, 6, and 7 introduce pseudo-asteroids to efficiently increase the size of the database. Once we find the optimal trajectory, we generate 10 pseudo-asteroids that spacecraft can fly by in the same trajectory. By introducing 10 pseudo-asteroids per each trajectory optimization, we can multiple the size of the database by $(1 + 10)$ with low computation time. For reference, Table 4 also shows the data generation speed using the parallel computation on a 3.0 GHz Intel Core i9 workstation with 18 cores/36 threads. Introducing pseudo-asteroids speeds up the computational time significantly and therefore increases the database size greatly.

As the post-process of the database generation, we remove outliers which do not satisfy the condition $0.5 < a < 10\text{au}$ and $\Delta V < 10\text{km/s}$, and apply the $\tan^{-1}(\cdot)$ operation to the outputs with $\Delta t_{f,90\%} = 30\text{ days}$, $\Delta v_{\infty,f,90\%} = 2\text{ km/s}$, and $\Delta V_{90\%} = 1\text{ km/s}$.

Figure 15 visualizes the databases for Case 1 and Case 7 with ΔV mapped to the asteroid orbital elements. The proposed method using pseudo-asteroids not only increases the size of the database, but also reduces the sparsity of the database that naturally exists in asteroid orbital dynamics.

C. Performance of Neural Network

This subsection shows the results of training DNNs on the database shown in the previous subsection. We use 90% of the databases as training data and 10% of them as validation data. Using a preliminary dataset independent of the datasets defined in Table 4, we first manually tune the hyperparameters of the networks and set the learning

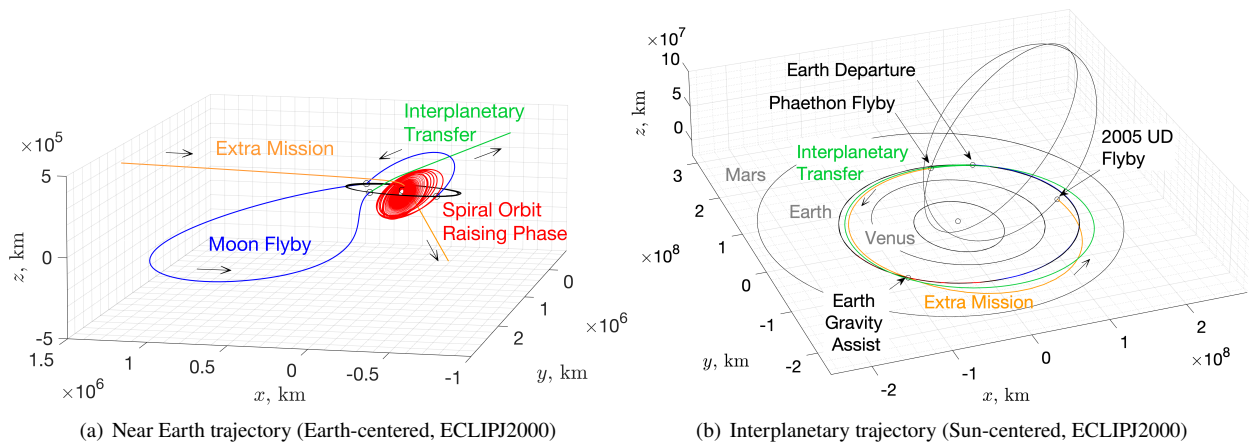


Fig. 14 DESTINY+baseline trajectory

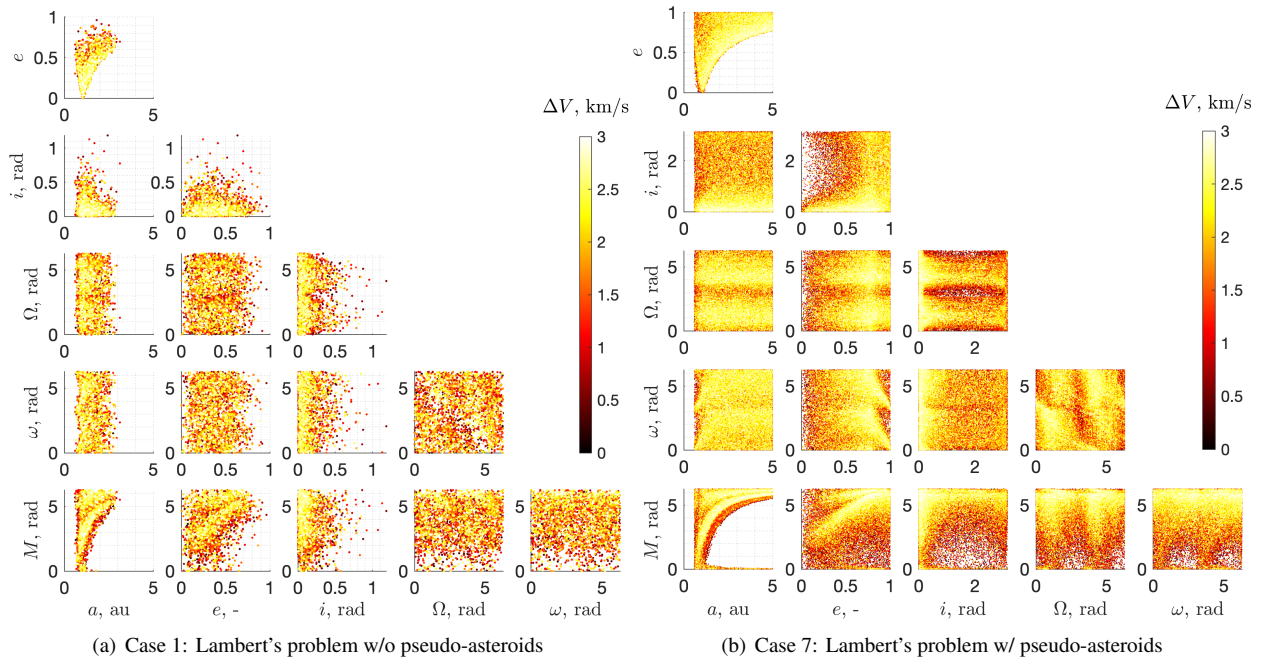


Fig. 15 ΔV plots of training databases (1:1 generic free-return trajectories).

Table 4 Definition of database

Case #	Screening algorithm	pseudo-asteroids	Size of database	Speed, sample/s
1	Lambert's problem	w/o pseudo-asteroids	698,368	8.77
2	Lambert's problem	w/ 10 pseudo-asteroids	698,368	47.6
3	Lambert's problem	w/ 10 pseudo-asteroids	6,983,680	47.6
4	Closest approach distance	w/o pseudo-asteroids	698,368	5.75
5	Closest approach distance	w/ 10 pseudo-asteroids	698,368	36.5
6	Closest approach distance	w/ 10 pseudo-asteroids	6,983,680	36.5
7	Lambert's problem	w/ 10 pseudo-asteroids	11,730,489	47.6

rate to $1e-4$, the number of layers to 5, and the number of units to 1,024 for all cases. The summary of the DNN performance is shown in Table 5, and the learning curves are illustrated in Appendix B. For the datasets of Cases 1, 2, 4, 5, DNNs with the batch normalization layer showed overfitting behavior, in which the validation loss deteriorated by more than one order of magnitude relative to the training loss. For these cases, introducing the dropout layer suppressed the overfitting behavior. On the other hand, applying the dropout layer worsened the validation loss compared to the batch normalization case. When the dataset size is larger than $7e6$, the overfitting does not occur even with the batch normalization. Thus, we apply the dropout layer for Cases 1, 2, 4, 5 and the batch normalization layer for Cases 3, 6, 7. This result demonstrates that at least $7e6$ datasets are needed to obtain practical performance for our application. Comparing Cases 1, 2, 4, 5, we observe that the performance is slightly better when the pseudo-asteroids are introduced, even if the size of the database is the same. Including the larger databases, Cases 3 and 6, we find that Case 3 records the best performance. Since Case 3 is the best condition, we create a more extensive database Case 7 with the same conditions as Case 3 except the size of the database. The learning curves of Case 7 are shown in Fig.16. Note that the total loss of Case 7 becomes $3.28e-4$ at epoch 4.5k. For reference, the computational speed is about 200,000 samples/s for each epoch using the GPU computation on a 3.0 GHz Intel Core i9 workstation with NVIDIA Quadro GV100 (32GB HBM2, Tensor 118.5Tflops). For Case 7, we performed an additional sensitivity analysis of the hyperparameters shown in Appendix C. Although we find better hyperparameters that reduce the validation loss, we perform the final evaluation using the parameters we initially set, considering validation loss and calculation speed of training and predicting.

Table 5 Performance of deep neural networks

Case #	Size of database	BN/DO	Validation loss (@epoch)
1	698,368	Drop Out	$2.26e-2$ (@1k)
2	698,368	Drop Out	$1.60e-2$ (@1k)
3	6,983,680	Batch Norm	$6.04e-4$ (@1k)
4	698,368	Drop Out	$1.70e-2$ (@1k)
5	698,368	Drop Out	$1.41e-2$ (@1k)
6	6,983,680	Batch Norm	$9.36e-3$ (@1k)
7	11,730,489	Batch Norm	$5.49e-4$ (@1k), $3.28e-4$ (@4.5k)

Figures 17 and 18 plot density heatmaps that illustrate the correlation between the estimated values and the true values. These density heatmaps are evaluated using 25,461 test trajectories (without pseudo-asteroids) that are independent of the DNNs training and validation process. Figure 17 compares the ΔV prediction performance of the DNN surrogate with Lambert's solution, typically used to estimate the optimal ΔV . The estimated ΔV by DNN and the true ΔV have a strong 1-to-1 correlation, whereas the Lambert's ΔV and the true ΔV have a weak correlation. The ΔV error magnitude of the DNN surrogates is about 0.1km/s or less, which is significantly improved from the typical Lambert's solution, as shown in Fig.17 (b). Figure 18 compares the DNN prediction performances of other outputs Δt_f and $\Delta v_{\infty, f}$. We also observe strong 1-to-1 correlations for both predictions.

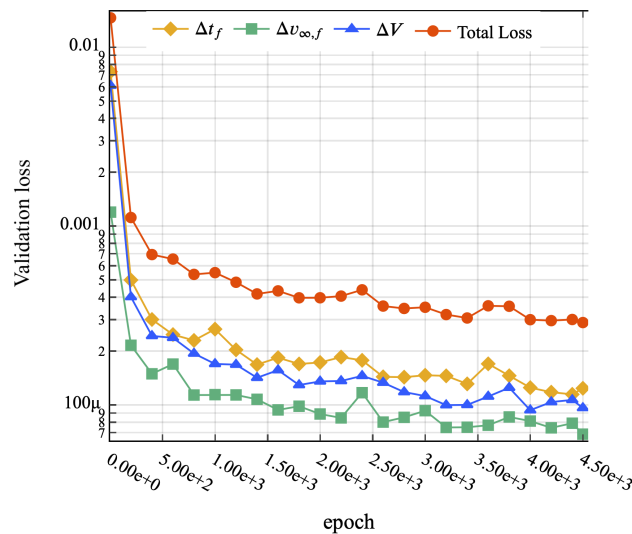


Fig. 16 Learning curve of best case (case 7).

D. Tree Search

Integrating the Earth-asteroid-Earth block with the DNN surrogate model, we search for good asteroid flyby sequences via beam search. The parameters to be searched in the beam search are the type of free-return trajectories and the orbital elements of the asteroids. The ephemerides of the target asteroids are acquired via the JPL small-body database search engine* under the condition of the perihelion radius $q \leq 1.4$ au, the aphelion radius $Q \geq 0.8$ au, and the OCC (Orbit Condition Code) ≤ 6 . As of July 22, 2021, the number of the target asteroids is 15,340.

Each parent has about 300,000 children in the tree search, and about 10,000 of them remain after the initial screening. The DNN surrogate evaluates the cost of 10,000 Earth-asteroid-Earth trajectories in 10 seconds, whereas the trajectory optimization takes about 1140 seconds for the same computation. Suppose that the beam width is 100 and the maximum depth is 5, the total computation time of our algorithm is about 10 hours, including initial screening and all pre/post-processing of database, whereas the trajectory optimization (without the DNN surrogate) is expected to take about 7 days for the same computation.

E. Patched Trajectory Optimization

Using the flyby sequence provided by the proposed method, we solve a multiple gravity-assist trajectory optimization problem that patches the whole trajectory. We patch each Earth-asteroid-Earth trajectory with an Earth gravity assist, modeled by a zero-radius sphere-of-influence patched-conics approach (e.g., [36, 37]). The gravity assist maneuver is modeled as an instantaneous velocity change with constraints on the hyperbolic excess velocity, deflection angle, and epoch of the Earth flyby between phases. We use the results of the DNN surrogate and the screening algorithms as the initial guess trajectories. This patched trajectory optimization was performed via a direct multiple shooting method that minimizes the total ΔV magnitude. The initial hyperbolic excess velocity and the Earth departure time are bounded with the ± 0.2 km/s and ± 7 days tolerance.

Table 6 shows some of the example patched asteroid flyby cyclers trajectories. We compare the total ΔV s between the DNN-based method and NLP-based patched trajectory optimization. The total ΔV of NLP differs from the predicted ΔV of DNNs because of the following factors. 1) Prediction errors of DNNs result in errors in ΔV , Earth gravity assist epoch, and hyperbolic excess velocity, as shown in Fig.17 (a), Fig.18 (a), and Fig.18 (b), respectively. Because the errors on the Earth gravity assist epoch and hyperbolic excess velocity change the boundary condition of the Earth-asteroid-Earth block, these errors are accumulated in the total ΔV for the patched trajectory optimization. For reference, as illustrated in Fig.17 (a), the ΔV error of the single-stage DNN surrogates (=Optimal ΔV by NLP – Estimated ΔV by DNN) is about 0.1km/s or less in most cases. The large error seen in ID1-0704 in Table 6 is likely because of this accumulation of errors in the Earth gravity assist epoch and hyperbolic excess velocity. 2) The patched trajectory optimization reduces the

*https://ssd.jpl.nasa.gov/sbdb_query.cgi (Accessed on July 22, 2021.)

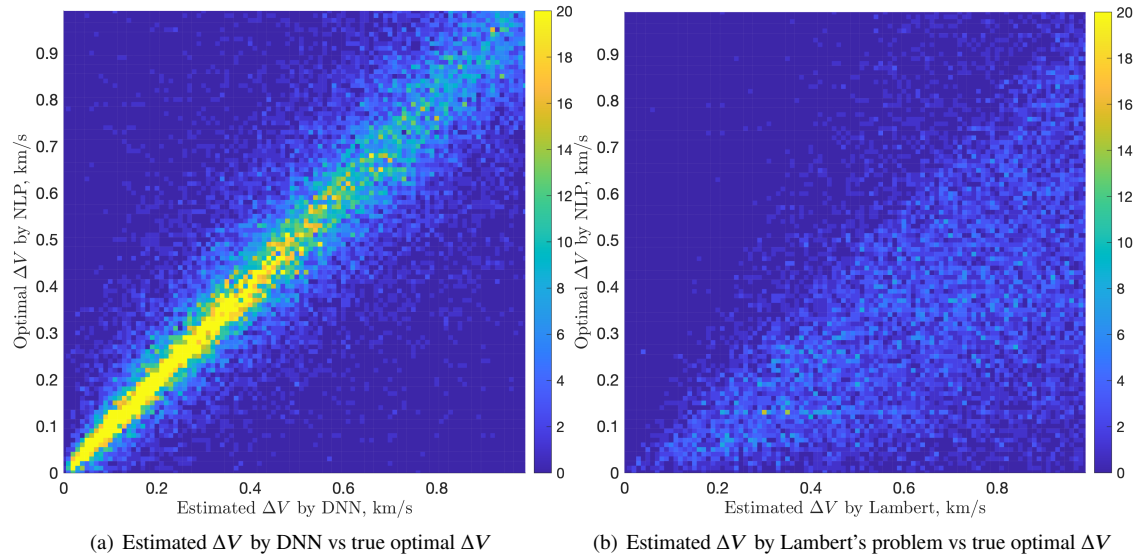


Fig. 17 Density heatmaps of the estimated ΔV s vs the true ΔV s (Color map: counts of the solution).

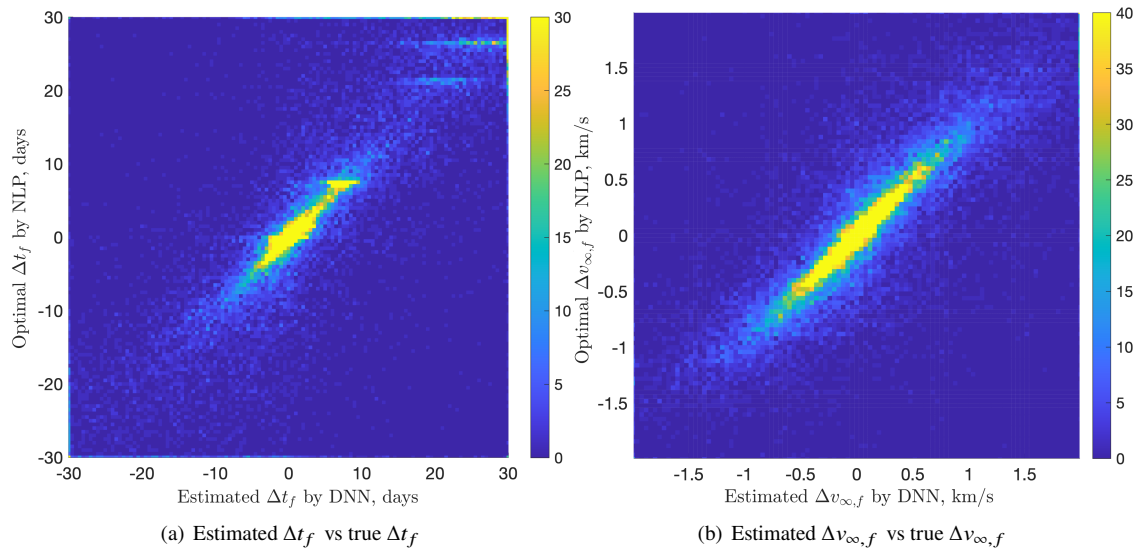


Fig. 18 Density heatmaps of the estimated outputs by DNNs vs the true outputs (Color map: counts of the solution).

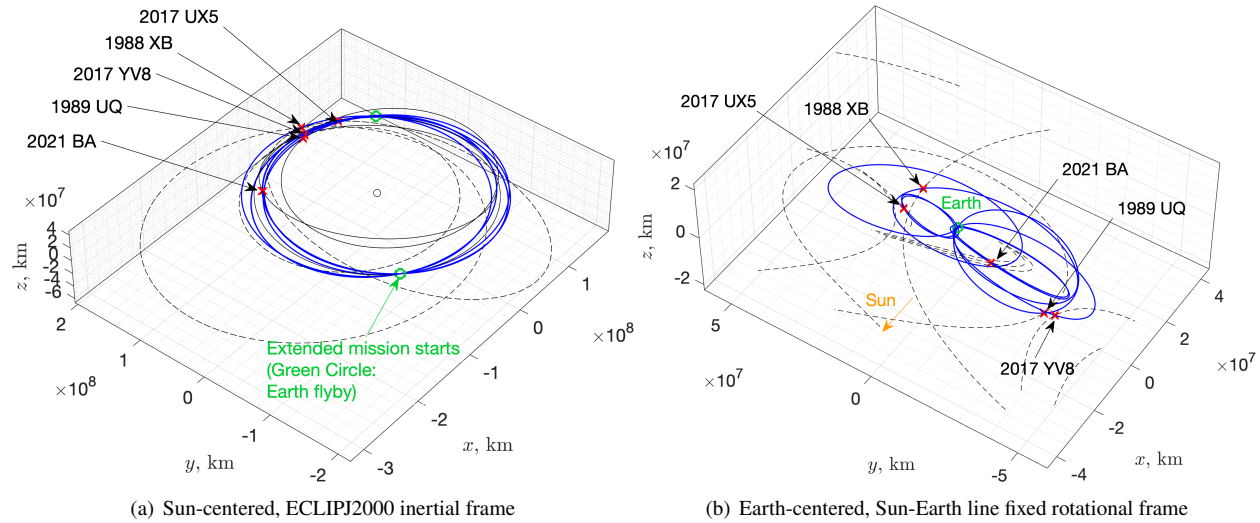


Fig. 19 ID 2-8373 asteroid flyby cyclers trajectory (nearly ballistic, long transfer time)

total ΔV consumption because the patched trajectory optimization solves the whole trajectory whereas the initial guess trajectory provided by DNNs is a sequence of optimal solutions to the subproblem in each Earth-asteroid-Earth block.

F. Example Solutions

This subsection shows the details of two example solutions. Two cases, ID 2-8373 and ID 1-1798, are presented as follows.

ID 2-8373 is a nearly ballistic solution that includes an exploration of two scientifically interesting B-type asteroids, which are thought to contain primitive and volatile-rich materials. Figure 19 shows the trajectories, and Table 7 summarizes the sequence of events. The spacecraft can fly by an asteroid every few years. The total ΔV of 65 m/s is affordable for micro spacecraft and CubeSats, such as PROCYON[46, 47] and EQUULEUS[48].

Table 7 Sequence of events for ID 2-8373

Date time, TDB	Event	v_∞ (Or v_{rel}), km/s	Perigee altitude, km	ΔV , km/s
2028 MAY 12 00:52:51	Earth flyby	2.567	232385	
2028 DEC 27 10:50:45	2017 YV8 flyby	10.063		
2029 MAY 12 07:05:22	Earth flyby	2.567	232386	
2030 FEB 10 00:45:50	2021 BA flyby	9.453		
2030 JUN 13 16:53:49	Deep space maneuver #1			0.0285
2031 MAY 12 14:49:00	Earth flyby	2.543	40380	
2031 DEC 26 19:28:45	1989 UQ flyby	6.501		
2033 MAY 12 03:13:28	Earth flyby	2.543	29185	
2033 NOV 12 10:58:02	2017 UX5 flyby	13.859		
2034 MAY 17 14:53:20	Deep space maneuver #2			0.0219
2035 MAY 12 15:40:17	Earth flyby	2.545	37295	
2036 JAN 30 23:48:10	Deep space maneuver #3			0.0141
2036 DEC 01 07:20:19	1988 XB flyby	11.423		
2037 OCT 31 20:46:55	Earth flyby	2.545	n/a	

ID 1-1798 is a short time transfer solution that includes an exploration of 2000 WO107, which is a contact binary

asteroid. Such an irregular-shaped asteroid is important to understand the collisional environment in the early solar system. Figure 20 shows the trajectories, and Table 8 summarizes the sequence of events. The spacecraft can fly by an asteroid almost every year. The total ΔV of 124 m/s is still reasonable for many missions.

Table 8 Sequence of events for ID 1-1798

Date time, TDB	Event	v_∞ (or v_{rel}), km/s	Perigee altitude, km	ΔV , km/s
2028 MAY 04 12:08:25	Earth flyby	2.691	11984	
2028 NOV 19 01:59:41	Deep space maneuver #1			0.0228
2028 NOV 23 07:49:22	1998 XX2 flyby	8.545		
2029 MAY 13 22:38:40	Deep space maneuver #2			0.0010
2029 NOV 03 09:26:10	Earth flyby	2.689	24795	
2030 MAY 17 15:23:49	2003 LN6 flyby	4.180		
2030 NOV 03 15:38:28	Earth flyby	2.689	297689	
2031 JUL 26 22:13:06	2016 JJ17 flyby	8.369		
2031 NOV 03 21:50:36	Earth flyby	2.689	1180355	
2032 FEB 05 07:41:40	Deep space maneuver #3			0.0169
2032 JUL 29 09:25:09	2005 QP11 flyby	4.054		
2032 NOV 03 21:37:26	Earth flyby	2.717	245400	
2033 AUG 11 07:23:50	Deep space maneuver #4			0.0835
2033 DEC 13 18:52:26	2000 WO107 flyby	28.477		
2034 APR 13 04:44:34	Earth flyby	2.779	n/a	

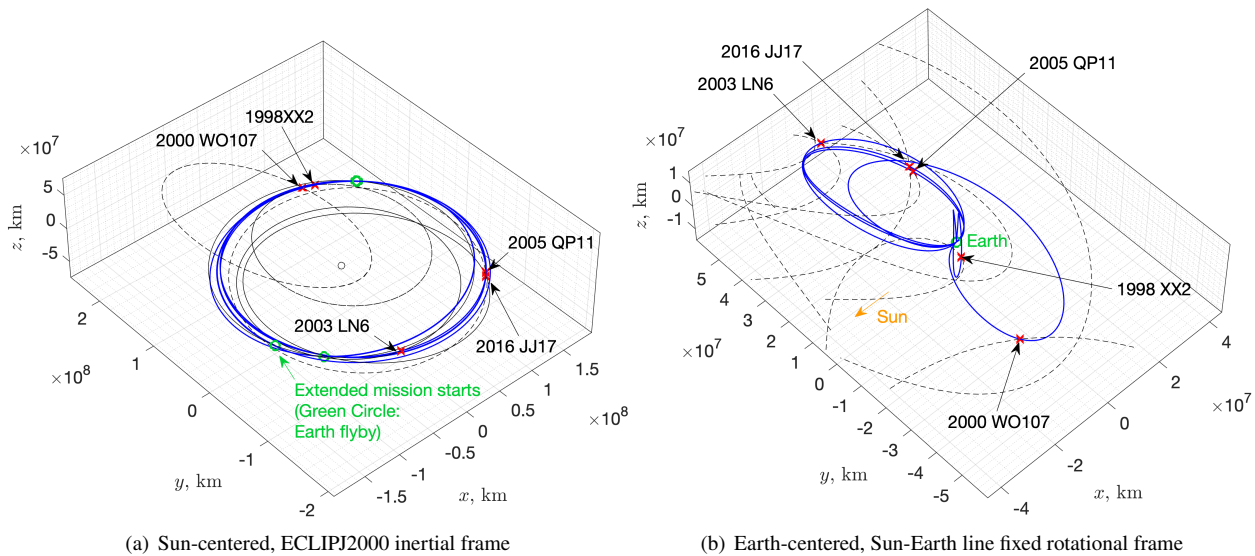


Fig. 20 ID 1-1798 asteroid flyby cyclers trajectory (short transfer time)

V. Conclusions

Asteroid flyby cyclers orbits allow for multiple asteroid flybys with little ΔV consumption. This paper proposes a novel trajectory design approach of asteroid flyby cyclers utilizing the surrogate model via deep neural networks. The proposed architecture creates the Earth-asteroid-Earth blocks integrating the surrogate model with astrodynamics knowledge, such as free-return trajectories and Lambert's problem, to improve the prediction accuracy. The resulting

surrogate models are reusable for different mission scenarios (different Earth departure epoch, hyperbolic excess velocity, and target asteroids) without re-training deep neural networks. Because machine learning-based trajectory design requires a computationally expensive gigantic database, we propose an efficient database generation strategy that can amplify the size of the optimal trajectory database by one order of magnitude by introducing pseudo-asteroids satisfying the Karush-Kuhn-Tucker conditions. These surrogate-based Earth-asteroid-Earth blocks allow us to search for good asteroid flyby sequences via beam search efficiently. The numerical application to JAXA's DESTINY⁺ mission, an upcoming asteroid flyby mission, shows that the proposed method is practically applicable to space mission design and efficiently finds the asteroid flyby cyclers trajectories.

Acknowledgments

This research is supported by the Adaptable and Seamless Technology Transfer Program (A-STEP) through Target-driven R&D, Grant Number JPMJTM20D9, from Japan Science and Technology Agency (JST). The first author would like to thank JAXA's DESTINY⁺ project team for their valuable comments.

Appendix A. Detail of Inputs of Deep Neural Network

This section explains the details of the input information of DNNs shown in Tables 2 and 3. Free-return info $(m, n, \text{type}, v_{\infty,0})$ and asteroid orbital elements $(a, e, i, \Delta\Omega_{t_0}, \omega, M_{t_0})$ are user-defined parameters, which are parametrically searched via tree search methods.

T is the time of flight of the free-return trajectory. n_{\star} is the number of revolutions of the spacecraft's orbit from Earth departure to the asteroid encounter. $\eta_{t_{\star}}$ is a parameter that determines the asteroid flyby epoch by the following equation.

$$\eta_{t_{\star}} = \frac{t_1 - t_0}{T}. \quad (\text{A.1})$$

$\mathbf{v}_{\infty,0}$, $\mathbf{v}_{\infty,f}$ and $\mathbf{v}_{\text{rel},1}$ are determined in the RSW frame with respect to the flyby body; the R axis is parallel to the position vector of the flyby body; the W axis is normal to the orbital plane of the flyby body; the S axis completes the right-handed system; \mathbf{e}_{FR} is the orbital element of the free-return trajectory calculated from $(m, n, \text{type}, v_{\infty,0})$.

We calculate ΔV s of Lambert's method as

$$\Delta v_0 = \|\mathbf{v}_{\infty\text{out},0}\| - v_{\infty,0} \quad (\text{A.2})$$

$$\Delta v_1 = \|\mathbf{v}_{\text{rel},\text{out},1} - \mathbf{v}_{\text{rel},\text{in},1}\| \quad (\text{A.3})$$

$$\Delta v_{\text{total}} = \Delta v_0 + \Delta v_1, \quad (\text{A.4})$$

and the closest approach state differences as

$$\delta \mathbf{r}_{\text{CA}} = R_z(-\lambda_{\oplus}(t_0)) (\mathbf{r}_{\text{sc},1} - \mathbf{r}_{\star}(t_1)) \quad (\text{A.5})$$

$$\delta \mathbf{v}_{\text{CA}} = R_z(-\lambda_{\oplus}(t_0)) (\mathbf{v}_{\text{sc},1} - \mathbf{v}_{\star}(t_1)) \quad (\text{A.6})$$

$$R_z(\theta) = \begin{bmatrix} \cos \theta & -\sin \theta & 0 \\ \sin \theta & \cos \theta & 0 \\ 0 & 0 & 1 \end{bmatrix}. \quad (\text{A.7})$$

Appendix B. Learning Curves for All Cases

Figures 21 illustrate the learning curves until 1k epoch for all cases. The definition of the corresponding database is written in Table 4. Case 7 records the best performance in all elements of the loss function.

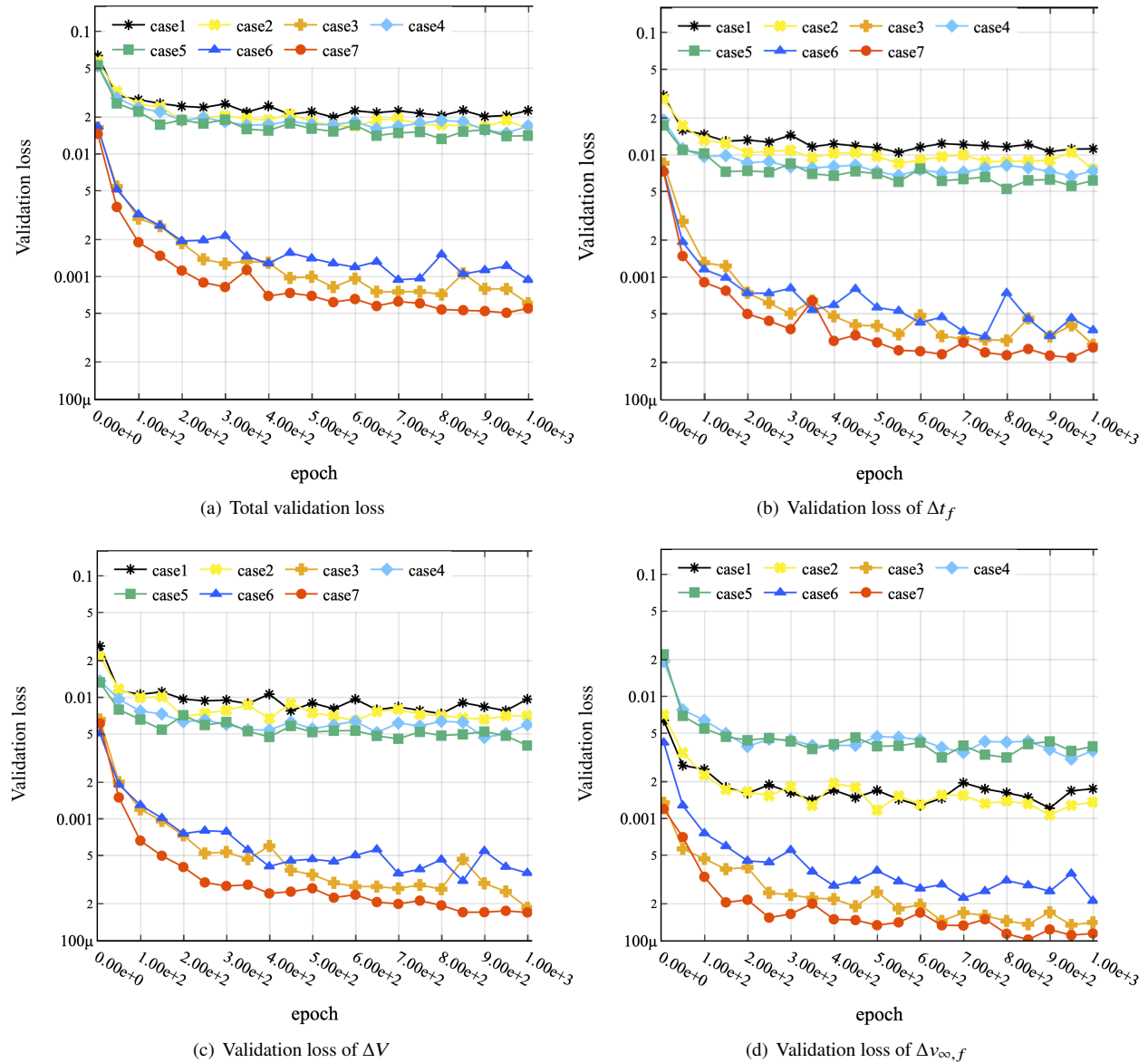
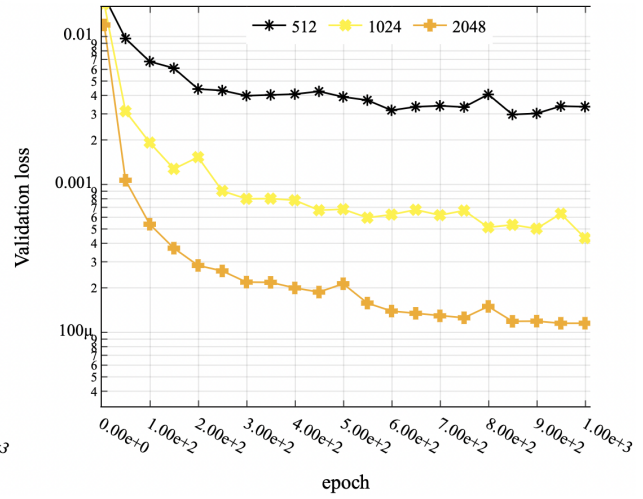
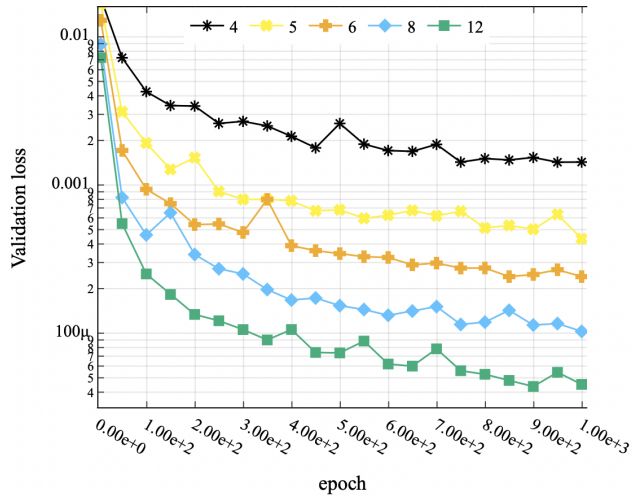


Fig. 21 Learning curve for all cases.

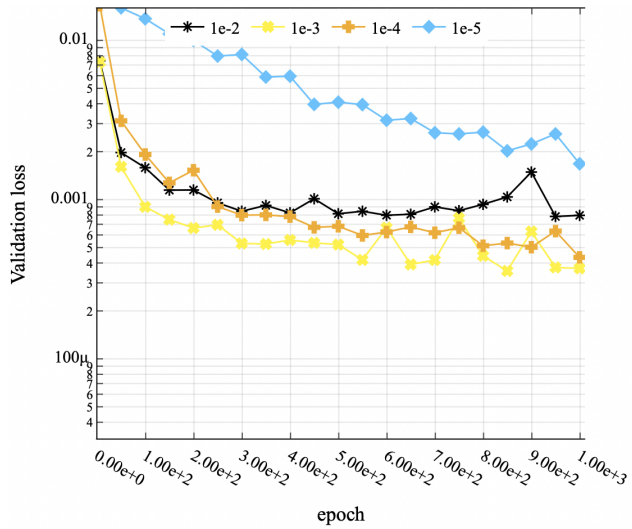
Appendix C. Sensitivity Analysis of Hyperparameters

We perform sensitivity analysis of the hyperparameters in the database of Case 7. Figures 22 illustrate the learning curves until 1k epoch for each hyperparameters. The summary of the learning results is written in Table 9. The calculation results show that Case 7-j gives the optimal hyperparameters that minimize the validation loss. The density heatmaps evaluated using the test data are shown in Figs.23 and 24. Although we found better hyperparameters that decrease the validation loss, we selected Case 7-a, considering validation loss and calculation speed of training and predicting. As for the learning rate shown in Fig.22 (c), we found that $1e-4$ converges more stably than $1e-3$, although the validation loss is slightly worse for $1e-4$ than for $1e-3$.



(a) Validation loss for each # of layers (# of units is 1024 and learning rate is $1e-4$)

(b) Validation loss for each # of units (# of layers is 5 and learning rate is $1e-4$)



(c) Validation loss for each learning rate (# of layers is 5 and # of units is 1024)

Fig. 22 Learning curve for each hyperparameters.

Table 9 Performance for each hyperparameter

Case #	# of Layers	# of Units	Learning rate	Validation loss (@epoch)	Speed (samples/s)
7-a	5	1024	1e-4	4.89e-4(@1k)	195,000
7-b	5	1024	1e-3	3.69e-4(@1k)	195,000
7-c	5	1024	1e-5	1.88e-3(@1k)	195,000
7-d	6	1024	1e-4	2.53e-4(@1k)	163,000
7-e	4	1024	1e-4	1.40e-3(@1k)	261,000
7-f	5	2048	1e-4	1.24e-4(@1k)	84,000
7-g	5	512	1e-4	3.36e-3(@1k)	168,000
7-h	5	1024	1e-2	9.98e-4(@1k)	195,000
7-i	8	1024	1e-4	1.10e-4(@1k)	115,000
7-j	12	1024	1e-4	4.44e-5(@1k), 2.46e-5(@3.2k)	74,000
7-k	6	2048	1e-4	5.76e-5(@1k)	64,000

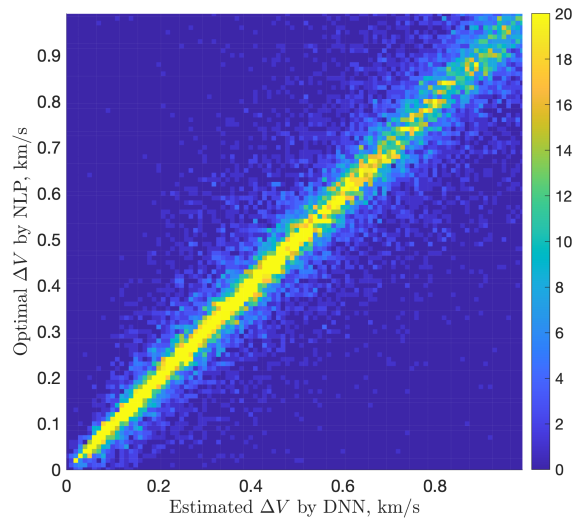


Fig. 23 Density heatmaps of the estimated ΔV s by DNNs vs the true optimal ΔV s (Color map: counts of the solution).

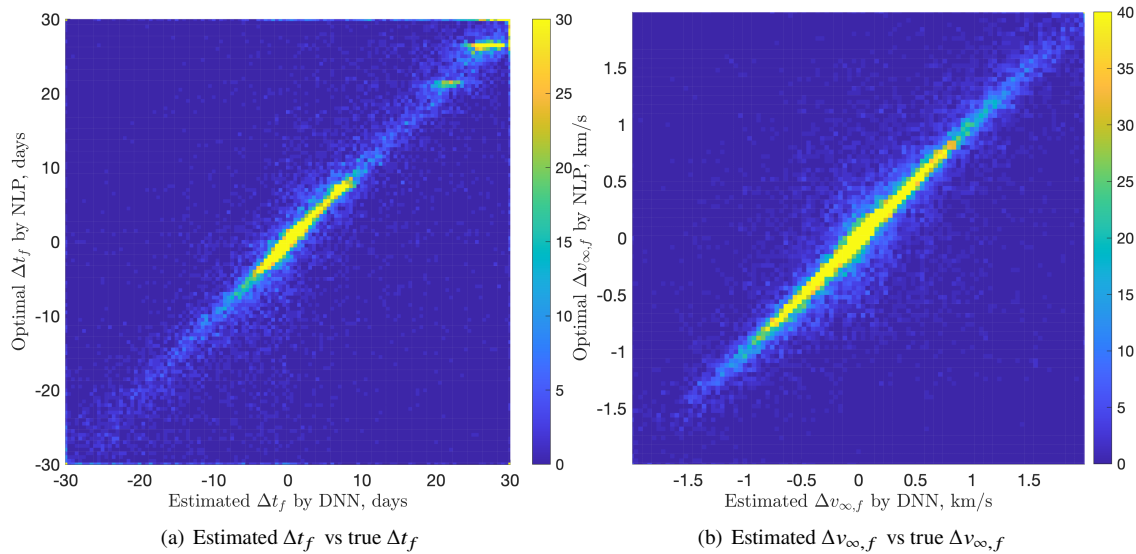


Fig. 24 Density heatmaps of the estimated outputs by DNNs vs the true outputs (Color map: counts of the solution).

References

- [1] Englander, J. A., Berry, K., Sutter, B., Stanbridge, D., Ellison, D. H., Williams, K., McAdams, J., Knittel, J. M., Welch, C., and Levison, H., "Trajectory design of the Lucy mission to explore the diversity of the Jupiter Trojans," *Proceedings of the International Astronautical Congress, IAC*, 2019, pp. 1–9. URL <https://ntrs.nasa.gov/citations/20190032357>.
- [2] Byrnes, D. V., Longuski, J. M., and Aldrin, B., "Cycler orbit between Earth and Mars," *Journal of Spacecraft and Rockets*, Vol. 30, No. 3, 1993, pp. 334–336. <https://doi.org/10.2514/3.25519>, URL <https://doi.org/10.2514/3.25519>.
- [3] Russell, R. P., and Ocampo, C. A., "Global Search for Idealized Free-Return Earth-Mars Cyclers," *Journal of Guidance, Control, and Dynamics*, Vol. 28, No. 2, 2005, pp. 194–208. <https://doi.org/10.2514/1.8696>, URL <https://doi.org/10.2514/1.8696>.
- [4] Russell, R. P., and Strange, N. J., "Cycler trajectories in planetary moon systems," *Journal of Guidance, Control, and Dynamics*, Vol. 32, No. 1, 2009, pp. 143–157. <https://doi.org/10.2514/1.36610>.
- [5] Campagnola, S., Buffington, B. B., Lam, T., Petropoulos, A. E., and Pellegrini, E., "Tour Design Techniques for the Europa Clipper Mission," *Journal of Guidance, Control, and Dynamics*, Vol. 42, No. 12, 2019, pp. 2615–2626. <https://doi.org/10.2514/1.G004309>, URL <https://doi.org/10.2514/1.G004309>.
- [6] Englander, J. A., Conway, B. A., and Williams, T., "Automated mission planning via evolutionary algorithms," *Journal of Guidance, Control, and Dynamics*, Vol. 35, No. 6, 2012, pp. 1878–1887. <https://doi.org/10.2514/1.54101>.
- [7] Englander, J. A., and Conway, B. A., "Automated solution of the low-thrust interplanetary trajectory problem," *Journal of Guidance, Control, and Dynamics*, Vol. 40, No. 1, 2017, pp. 15–27. <https://doi.org/10.2514/1.G002124>.
- [8] Petropoulos, A., Grebow, D., Jones, D., Lantoine, G., Nicholas, A., Roa, J., Senent, J., Stuart, J., Arora, N., Pavlak, T., Lam, T., McElrath, T., Roncoli, R., Garza, D., Bradley, N., Landau, D., Tarzi, Z., Laipert, F., Bonfiglio, E., Wallace, M., and Sims, J., "GTOC9: Results from the Jet Propulsion Laboratory (team JPL)," *Acta Futura*, 2018, pp. 25–35. <https://doi.org/10.5281/zenodo.1139152>.
- [9] Di Carlo, M., Vasile, M., and Dunlop, J., "Low-thrust tour of the main belt asteroids," *Advances in Space Research*, Vol. 62, No. 8, 2018, pp. 2026–2045. <https://doi.org/https://doi.org/10.1016/j.asr.2017.12.033>, URL <https://www.sciencedirect.com/science/article/pii/S0273117717309213>.
- [10] Olympio, J. T., "Optimal Control Problem for Low-Thrust Multiple Asteroid Tour Missions," *Journal of Guidance, Control, and Dynamics*, Vol. 34, No. 6, 2011, pp. 1709–1720. <https://doi.org/10.2514/1.53339>.

- [11] Grigoriev, I., and Zapletin, M., "Choosing promising sequences of asteroids," *Automation and Remote Control*, Vol. 74, 2013, pp. 1284–1296. <https://doi.org/10.1134/S0005117913080055>.
- [12] Sánchez Cuartielles, J., Gibbings, A., Snodgrass, C., Green, S., and Bowles, N., "Asteroid belt multiple flyby options for M-Class Missions," *67th International Astronautical Congress, IAC-2016*, Guadalajara, Mexico, 2016. URL <https://dspace.lib.cranfield.ac.uk/handle/1826/10874>.
- [13] Bowles, N., Snodgrass, C., Gibbings, A., Sanchez, J., Arnold, J., Eccleston, P., Andert, T., Probst, A., Naletto, G., Vandaele, A., de Leon, J., Nathues, A., Thomas, I., Thomas, N., Jorda, L., Da Deppo, V., Haack, H., Green, S., Carry, B., Donaldson Hanna, K., Leif Jorgensen, J., Kereszturi, A., DeMeo, F., Patel, M., Davies, J., Clarke, F., Kinch, K., Guilbert-Lepoutre, A., Agarwal, J., Rivkin, A., Pravec, P., Fornasier, S., Granvik, M., Jones, R., Murdoch, N., Joy, K., Pascale, E., Tecza, M., Barnes, J., Licandro, J., Greenhagen, B., Calcutt, S., Marriner, C., Warren, T., and Tosh, I., "CASTAway: An asteroid main belt tour and survey," *Advances in Space Research*, Vol. 62, No. 8, 2018, pp. 1998–2025. <https://doi.org/https://doi.org/10.1016/j.asr.2017.10.021>, URL <https://www.sciencedirect.com/science/article/pii/S0273117717307597>, past, Present and Future of Small Body Science and Exploration.
- [14] Haftka, R. T., Villanueva, D., and Chaudhuri, A., "Parallel surrogate-assisted global optimization with expensive functions – a survey," *Structural and Multidisciplinary Optimization*, Vol. 54, No. 1, 2016, pp. 3–13. <https://doi.org/10.1007/s00158-016-1432-3>.
- [15] Brochu, E., Cora, V. M., and de Freitas, N., "A Tutorial on Bayesian Optimization of Expensive Cost Functions, with Application to Active User Modeling and Hierarchical Reinforcement Learning," 2010. URL <http://arxiv.org/abs/1012.2599>.
- [16] Snoek, J., Larochelle, H., and Adams, R. P., "Practical Bayesian optimization of machine learning algorithms," *Advances in Neural Information Processing Systems*, Vol. 4, 2012, pp. 2951–2959. <https://doi.org/https://dl.acm.org/doi/10.5555/2999325.2999464>, URL <https://dl.acm.org/doi/10.5555/2999325.2999464>.
- [17] Jin, Y., "Surrogate-assisted evolutionary computation: Recent advances and future challenges," *Swarm and Evolutionary Computation*, Vol. 1, No. 2, 2011, pp. 61–70. <https://doi.org/10.1016/j.swevo.2011.05.001>.
- [18] Parno, M. D., Hemker, T., and Fowler, K. R., "Applicability of surrogates to improve efficiency of particle swarm optimization for simulation-based problems," *Engineering Optimization*, Vol. 44, No. 5, 2012, pp. 521–535. <https://doi.org/10.1080/0305215X.2011.598521>.
- [19] Yang, H., Yan, J., and Li, S., "Fast computation of the Jovian-moon three-body flyby map based on artificial neural networks," *Acta Astronautica*, 2021. <https://doi.org/https://doi.org/10.1016/j.actaastro.2021.08.054>, URL <https://www.sciencedirect.com/science/article/pii/S0094576521004756>.
- [20] Yang, B., Li, S., Feng, J., and Vasile, M., "Fast Solver for J2-Perturbed Lambert Problem Using Deep Neural Network," *Journal of Guidance, Control, and Dynamics*, Vol. 0, No. 0, 0, pp. 1–10. <https://doi.org/10.2514/1.G006091>, URL <https://doi.org/10.2514/1.G006091>.
- [21] Izzo, D., Märten, M., and Pan, B., "A survey on artificial intelligence trends in spacecraft guidance dynamics and control," *Astrodynamics*, Vol. 3, 2019, pp. 287–299. <https://doi.org/https://doi.org/10.1007/s42064-018-0053-6>.
- [22] Hennes, D., Izzo, D., and Landau, D., "Fast approximators for optimal low-thrust hops between main belt asteroids," *2016 IEEE Symposium Series on Computational Intelligence, SSCI 2016*, 2017. <https://doi.org/10.1109/SSCI.2016.7850107>.
- [23] Mereta, A., Izzo, D., and Wittig, A., "Machine Learning of Optimal Low-thrust Transfers between Near-Earth Objects," *Hybrid Artificial Intelligent Systems*, 2017, pp. 543–553. https://doi.org/https://doi.org/10.1007/978-3-319-59650-1_46.
- [24] Shang, H., and Liu, Y., "Assessing Accessibility of Main-Belt Asteroids Based on Gaussian Process Regression," *Journal of Guidance, Control, and Dynamics*, Vol. 40, No. 5, 2017, pp. 1144–1154. <https://doi.org/10.2514/1.G000576>.
- [25] Shang, H., Wu, X., Qiao, D., and Huang, X., "Parameter estimation for optimal asteroid transfer trajectories using supervised machine learning," *Aerospace Science and Technology*, Vol. 79, 2018, pp. 570–579. <https://doi.org/10.1016/j.ast.2018.06.002>.
- [26] Viavattene, G., and Ceriotti, M., "Artificial Neural Networks for Multiple NEA Rendezvous Missions with Continuous Thrust," *Journal of Spacecraft and Rockets*, Vol. 0, No. 0, 0, pp. 1–13. <https://doi.org/10.2514/1.A34799>.
- [27] Li, H., Chen, S., Izzo, D., and Baoyin, H., "Deep networks as approximators of optimal low-thrust and multi-impulse cost in multitarget missions," *Acta Astronautica*, Vol. 166, 2020, pp. 469–481. <https://doi.org/https://doi.org/10.1016/j.actaastro.2019.09.023>.

- [28] Zhu, Y.-h., and Luo, Y.-Z., "Fast Evaluation of Low-Thrust Transfers via Multilayer Perceptions," *Journal of Guidance, Control, and Dynamics*, Vol. 42, No. 12, 2019, pp. 2627–2637. <https://doi.org/10.2514/1.G004080>, URL <https://doi.org/10.2514/1.G004080>.
- [29] Izzo, D., and Öztürk, E., "Real-Time Guidance for Low-Thrust Transfers Using Deep Neural Networks," *Journal of Guidance, Control, and Dynamics*, Vol. 44, No. 2, 2021, pp. 315–327. <https://doi.org/10.2514/1.G005254>, URL <https://doi.org/10.2514/1.G005254>.
- [30] Russell, R. P., and Ocampo, C. A., "Geometric analysis of free-return trajectories following a gravity-assisted flyby," *Journal of Spacecraft and Rockets*, Vol. 42, No. 1, 2005, pp. 138–151. <https://doi.org/10.2514/1.5571>.
- [31] Prussing, J. E., "A class of optimal two-impulse rendezvous using multiple-revolution Lambert solutions," *Journal of the Astronautical Sciences*, Vol. 48, No. 2-3, 2000, pp. 131–148. <https://doi.org/10.1007/bf03546273>.
- [32] Shen, H., and Tsiotras, P., "Using Battin's Method To Obtain Multiple-Revolution Lambert's S Solutions," *Advances in the Astronautical Sciences*, , No. 757, 2004, pp. 1–18. URL <https://citeseerx.ist.psu.edu/viewdoc/summary?doi=10.1.1.72.8486>.
- [33] Izzo, D., "Revisiting Lambert's problem," *Celestial Mechanics and Dynamical Astronomy*, Vol. 121, 2015, pp. 1–15. <https://doi.org/10.1007/s10569-014-9587-y>.
- [34] Izzo, D., Hennes, D., Simões, L. F., and Märten, M., *Designing Complex Interplanetary Trajectories for the Global Trajectory Optimization Competitions*, Springer International Publishing, Cham, 2016, pp. 151–176. https://doi.org/10.1007/978-3-319-41508-6_6, URL https://doi.org/10.1007/978-3-319-41508-6_6.
- [35] Ozaki, N., Yamamoto, T., Gonzalez-Franquesa, F., Gutierrez-Ramon, R., Pushparaj, N., Chikazawa, T., Dei Tos, D. A., Çelik, O., Marmo, N., Kawakatsu, Y., Arai, T., Nishiyama, K., and Takashima, T., "Mission Design of DESTINY+: Toward Active Asteroid (3200) Phaethon and Multiple Small Bodies," *arXiv*, 2022. URL <https://arxiv.org/abs/2201.01933>.
- [36] Vasile, M., and De Pascale, P., "Preliminary Design of Multiple Gravity-Assist Trajectories," *Journal of Spacecraft and Rockets*, Vol. 43, No. 4, 2006, pp. 794–805. <https://doi.org/10.2514/1.17413>, URL <https://doi.org/10.2514/1.17413>.
- [37] Ozaki, N., Oguri, K., and Funase, R., "PROCYON Mission Reanalysis: Low-Thrust Asteroid Flyby Trajectory Design leveraging Convex Programming," *The Journal of the Astronautical Sciences*, 2022. <https://doi.org/https://doi.org/10.1007/s40295-021-00299-4>.
- [38] Vinkó, T., and Izzo, D., "Global Optimisation Heuristics and Test Problems for Preliminary Spacecraft Trajectory Design," *ESA TR GOHTPPSTD*, 2008. URL <https://www.esa.int/gsp/ACT/doc/INF/pub/ACT-TNT-INF-2008-GOHTPPSTD.pdf>.
- [39] Strange, N., Russell, R., and Buffington, B., "Mapping the V-infinity globe," *Advances in the Astronautical Sciences*, Vol. 129, 2007. URL <http://www.univelt.com/book=1802>.
- [40] Gill, P. E., Murray, W., and Saunders, M. A., "SNOPT: An SQP algorithm for large-scale constrained optimization," *SIAM Rev.*, Vol. 47, 2005, pp. 99–131. <https://doi.org/https://doi.org/10.1137/S0036144504446096>.
- [41] Clevert, D.-A., Unterthiner, T., and Hochreiter, S., "Fast and Accurate Deep Network Learning by Exponential Linear Units (ELUs)," *arXiv*, 2015. URL <https://arxiv.org/abs/1511.07289>.
- [42] Ioffe, S., and Szegedy, C., "Batch Normalization: Accelerating Deep Network Training by Reducing Internal Covariate Shift," *Proceedings of the 32nd International Conference on International Conference on Machine Learning - Volume 37*, JMLR.org, 2015, p. 448–456. <https://doi.org/https://dl.acm.org/doi/10.5555/3045118.3045167>.
- [43] Kingma, D. P., and Ba, J., "Adam: A Method for Stochastic Optimization," *arXiv*, 2014. URL <https://arxiv.org/abs/1412.6980>.
- [44] Sarli, B. V., Kawakatsu, Y., and Arai, T., "Design of a Multiple Flyby Mission to the Phaethon–Geminid Complex," *Journal of Spacecraft and Rockets*, Vol. 52, No. 3, 2015, pp. 739–745. <https://doi.org/10.2514/1.A33130>, URL <https://doi.org/10.2514/1.A33130>.
- [45] Çelik, O., Dei Tos, D. A., Yamamoto, T., Ozaki, N., Kawakatsu, Y., and Yam, C. H., "Multiple-Target Low-Thrust Interplanetary Trajectory of DESTINY+," *Journal of Spacecraft and Rockets*, Vol. 58, No. 3, 2021, pp. 830–847. <https://doi.org/10.2514/1.A34804>.
- [46] Campagnola, S., Ozaki, N., Sugimoto, Y., Yam, C. H., Hongru, C., Kawabata, Y., Ogura, S., Sarli, B., Kawakatsu, Y., Funase, R., and Nakasuka, S., "Low-Thrust Trajectory Design and Operations of PROCYON, The First Deep-space Micro-spacecraft," *25th International Symposium on Space Flight Dynamics*, 2015, pp. 1–14. URL https://issfd.org/2015/files/downloads/papers/072_Campagnola.pdf.

- [47] Funase, R., Inamori, T., Ikari, S., Ozaki, N., Koizumi, H., Tomiki, A., Kobayashi, Y., and Kawakatsu, Y., "Initial Operation Results of a 50kg-class Deep Space Exploration Micro-Spacecraft PROCYON," *AIAA/USU Small Satellite Conference*, 2015. URL <https://digitalcommons.usu.edu/smallsat/2015/all2015/34/>.
- [48] Campagnola, S., Hernando-Ayuso, J., Kakihara, K., Kawabata, Y., Chikazawa, T., Funase, R., Ozaki, N., Baresi, N., Hashimoto, T., Kawakatsu, Y., Ikenaga, T., Oguri, K., and Oshima, K., "Mission Analysis for the EM-1 CubeSats EQUULEUS and OMOTENASHI," *IEEE Aerospace and Electronic Systems Magazine*, Vol. 34, No. 4, 2019, pp. 38–44. <https://doi.org/10.1109/MAES.2019.2916291>.

Table 6 List of example patched asteroid flyby cyclers trajectories

ID	Total ΔV , km/s		Total TOF, year		Free-return info		Target body info
	DNN	NLP	DNN	NLP	Leg	Type (m:n, $V_{\infty, \text{EGA0}}$ km/s)	Name (H, OCC, PHA, SMASSII spec.)
2-3094	0.1850	0.05101	9.488	9.507	1	full (2:2, 2.706)	2000 MU1 (19.88, 0, Y, S)
					2	full (2:2, 2.706)	2005 VQ96 (20.4, 0, Y, -)
					3	full (2:2, 2.708)	2019 RC2 (22.5, 6, N, -)
					4	full (2:2, 2.714)	2016 GU (25.7, 6, N, -)
					5	generic (1:1, 2.719)	2000 AC6 (21.5, 0, Y, Q)
2-0866	0.09012	0.06208	5.993	5.996	1	full (1:1, 2.764)	2017 AE5 (22.3, 0, N, -)
					2	full (1:1, 2.764)	2014 UU56 (28.6, 6, N, -)
					3	full (1:1, 2.788)	2016 QE45 (21.78, 0, Y, -)
					4	full (2:2, 2.751)	2013 CY (28.3, 5, N, -)
					5	full (1:1, 2.751)	Vishnu (18.32, 0, Y, O)
2-8373	0.09739	0.06446	9.488	9.479	1	full (1:1, 2.567)	2017 YV8 (27.3, 5, N, -)
					2	full (2:2, 2.567)	2021 BA (26.01, 6, N, -)
					3	full (2:2, 2.543)	1989 UQ (19.5, 0, Y, B)
					4	full (2:2, 2.543)	2017 UX5 (19.8, 2, Y, -)
					5	generic (2:2, 2.545)	1988 XB (17.96, 0, Y, B)
2-4497	0.1996	0.1139	9.014	9.010	1	full (2:2, 2.535)	2017 UX5 (19.8, 2, Y, -)
					2	full (2:2, 2.536)	1999 MN (21.15, 0, Y, -)
					3	full (2:2, 2.550)	2017 UX5 (19.8, 2, Y, -)
					4	full (2:2, 2.550)	2021 FC (28.25, 4, N, -)
					5	full (1:1, 2.442)	2013 WT67 (17.98, 0, Y, U)
1-1798	0.2101	0.1242	5.956	5.944	1	half (1.5:1.5, 2.691)	1998 XX2 (19.9, 0, Y, -)
					2	full (1:1, 2.689)	2003 LN6 (24.6, 2, N, -)
					3	full (1:1, 2.689)	2016 JJ17 (22.9, 3, N, -)
					4	full (1:1, 2.689)	2005 QP11 (26.4, 4, N, -)
					5	generic (1:1, 2.717)	2000 WO107 (19.28, 0, Y, X)
1-0160	0.1682	0.1655	5.994	5.997	1	full (1:1, 2.785)	2017 AE5 (22.3, 0, N, -)
					2	full (1:1, 2.785)	2014 UU56 (28.6, 6, N, -)
					3	half (1.5:1.5, 2.745)	2000 WF3 (23.4, 4, N, -)
					4	full (1:1, 2.734)	2020 OB6 (24.9, 5, N, -)
					5	half (1.5:1.5, 2.734)	1996 EN (16.39, 0, Y, U)
2-0587	0.1611	0.2589	9.477	9.511	1	full (2:2, 2.551)	2021 GB8 (27.36, 6, N, -)
					2	full (2:2, 2.551)	2014 KG39 (25, 3, N, -)
					3	full (2:2, 2.551)	2019 TE3 (25.5, 6, N, -)
					4	full (2:2, 2.581)	2017 KB3 (25.1, 6, N, -)
					5	generic (1:1, 2.581)	P/2016 BA14 PANSTARRS (-, 1, -, -)
1-0704	0.08417	0.3204	4.992	4.998	1	full (1:1, 2.798)	2017 AE5 (22.3, 0, N, -)
					2	full (1:1, 2.798)	2014 UU56 (28.6, 6, N, -)
					3	full (1:1, 2.755)	2017 WX13 (24.4, 6, N, -)
					4	full (1:1, 2.755)	2006 CJ (20.2, 0, Y, -)
					5	full (1:1, 2.733)	Midas (15.22, 0, Y, V)